RESEARCH ARTICLE

Subunit-specific roles of LRRC8 proteins in determining glutamate permeability of astrocytic volume-regulated anion channels

Madison L. Chandler, Ariella D. Sprague, Julia W. Nalwalk, and Alexander A. Mongin*

Department of Neuroscience and Experimental Therapeutics, Albany Medical College, Albany, New York, United States

*Correspondence: A.A. Mongin (mongina@amc.edu)

Running Head: COMPOSITION OF ASTROCYTIC LRRC8/VRAC CHANNELS

ABSTRACT

Volume-regulated anion channels (VRACs) are ubiquitous chloride channels that play a crucial role in cell volume regulation but are also involved in many other physiological processes. VRACs are heteromers of proteins from the leucine-rich repeat-containing family 8 (LRRC8A–E), with LRRC8A being essential. Other LRRC8 subunits are expressed in a cell type-specific manner and modulate the biophysical properties of VRACs, including permeability to small signaling molecules. Here, we used primary astrocyte cultures from wild-type and genetically modified C57BL/6 mice to investigate (i) LRRC8 subunit composition of endogenous VRACs in the brain and (ii) the subunit determinants of VRAC permeability to the excitatory neurotransmitter glutamate. qPCR and RNA-seq revealed high expression of *Lrrc8a–d* in mouse forebrain and astrocytes. As expected, *Lrrc8a* deletion abolished VRAC activity, measured as swelling-activated release of the glutamate analogue D-[^{3}H]aspartate. RNAi knockdown of individual subunits established that LRRC8A and LRRC8C are key components of astrocytic glutamate-permeable VRACs, with their siRNAs reducing radiotracer release by 85% and 56%, respectively. Downregulation of LRRC8D had a moderate effect, which depended on the severity of swelling. Combined silencing of LRRC8C and LRRC8D suggested that these subunits act in distinct channel populations. LRRC8B silencing alone was ineffective but partially rescued glutamate release in LRRC8C- or LRRC8D-knockdown cells. Overall, these findings indicate that astrocytic glutamate-permeable VRACs are primarily composed of LRRC8A and LRRC8C, with a possible structural role for LRRC8B. The refined understanding of VRAC subunit composition may inform the development of targeted VRAC inhibitors to mitigate glutamate excitotoxicity in neurological disorders.

NEW & NOTEWORTHY

We examined the subunit composition of volume-regulated anion channels (VRACs), which contribute to pathological glutamate release in various neurological disorders. VRACs are heteromers formed by LRRC8A–E proteins, but the subunit configuration and functional roles within native channels remain poorly understood. In mouse astrocytes, we determined that glutamate-permeable VRACs are composed primarily of LRRC8A and LRRC8C, with structural support from LRRC8B. These findings provide a foundation for developing subunit-specific VRAC inhibitors as potential neuroprotective therapies.

Keywords: Astrocytes, Glutamate release, LRRC8, LRRC8A, VRAC

INTRODUCTION

Volume-regulated anion channels (VRACs), also known as volume-sensitive outwardly rectifying anion channels (VSOR) or volume-sensitive organic osmolyte/anion channels (VSOAC), are swelling-activated chloride (Cl^-) channels found in virtually all vertebrate cells (1-3). VRAC activity is typically assessed by measuring swelling-induced Cl^- currents ($I_{Cl,vol}$) in cells exposed to hypoosmotic media [e.g., early studies (4-7)]. However, in addition to Cl^-, VRACs are also permeable to a range of small negatively charged or uncharged organic molecules, collectively referred to as organic osmolytes (1, 8-11). As their name implies, VRACs play a key role in cell volume control and drive regulatory volume decrease (RVD), a fundamental physiological process that restores cell volume after osmotic swelling. RVD is driven primarily by the electrically coupled efflux of cytosolic Cl^- (via VRACs) and K^+ (via separate K^+ channels), with additional contributions from bicarbonate and organic osmolytes (1-3). Beyond their role in RVD, VRACs have been implicated in numerous other physiological and pathological processes, including regulation of membrane potential, cell proliferation, apoptosis, immune responses, and paracrine signaling [reviewed in (12-16)].

In the context of brain physiology, VRACs are thought to exert a strong influence over the physiological and pathological regulation of brain excitability [reviewed in (13, 17-19)]. This unique role is due to VRACs' permeability to several amino acid-derived neurotransmitters and neuromodulators, including aspartate, glutamate, GABA, and taurine (8, 20, 21). Hence, once open, these channels have considerable potential to affect electrical activity in neural networks (16). VRACs' influence becomes even more pronounced in neural pathologies that promote pathological cell swelling, such as stroke, traumatic brain injury, and epilepsy. In these disorders, swelling-induced activation of VRACs leads to the release of cytosolic glutamate and contributes to excitotoxic neuronal damage (17, 22, 23). In mouse, rat, and canine models of stroke, the putative but structurally diverse VRAC blockers—tamoxifen, DCPIB, dicoumarol, and broma-diolone—potently reduce pathological glutamate release and ischemic brain infarction with a considerable therapeutic window of up to 3 hours after the interruption of blood flow (24-28). However, none of the currently available small molecule inhibitors possess sufficient specificity to confirm that their neuroprotective effects are mediated exclusively through inhibition of VRAC. For nearly three decades, the unknown molecular identity of VRACs has hindered progress in understanding their diverse roles in the brain as well as their potential as a therapeutic target [for a historical perspective, see (29-31)].

In 2014, the laboratories of Ardem Patapoutian and Thomas J. Jentsch independently solved the long-standing enigma of VRAC identity. Using genome-wide siRNA screens combined with a high-throughput YFP quenching assay to measure Cl^- permeability, they identified leucine-rich repeat-containing family 8 member A (LRRC8A, also known as Swell1) as an essential VRAC component (32, 33). LRRC8A belongs to a family of five LRRC8 proteins (LRRC8A-E), which share high sequence homology and a common evolutionary origin with vertebrate pannexins (34). Subsequent studies in CRISPR/Cas9-edited cells further established that LRRC8A must heteromerize with at least one other isoform, LRRC8C, LRRC8D, or LRRC8E, to form a fully functional channel (33, 35). Interestingly, LRRC8A/LRRC8B heteromers remain functionally silent for reasons that are not fully understood (33). Based on the structural homology with pannexins, LRRC8 proteins were predicted to assemble into hexamers with one central ion-conducting pore (34). The hexameric model of VRAC has been confirmed by multiple cryo-electron microscopy (cryo-EM) studies (36-39). However, more recent cryo-EM work indicates that LRRC8 channels can also adopt an alternative heptameric stoichiometry, such as LRRC8C homo-heptamers (40, 41).

The discovery of the indispensable role of LRRC8A has enabled the use of molecular genetics strategies to study the physiological role of VRACs. The Geha laboratory produced the first global LRRC8A knockout (KO) (42) to investigate a clinical case of congenital agammaglobulinemia, a severe immunoglobulin deficiency due to the loss of B lymphocytes, in a patient with a C-terminal truncation of LRRC8A (43). Unexpectedly, LRRC8A KO mice developed a lethal phenotype: ~80% of them died in utero, with the surviving animals rapidly dying due to multi-organ failure (42). In contrast, tissue- and cell type-specific LRRC8A deletions are generally better tolerated. For example, mice with conditional deletion of LRRC8A in CNS astrocytes show normal brain development and remain viable and fertile (44). However, astrocytic LRRC8A KO resulted in altered neuronal communication and deficits in learning and memory, likely due to reduced astrocytic glutamate release and consequent decreased activation of neuronal glutamate receptors (44). In another study, astrocytic VRACs were shown to mediate tonic release of the inhibitory neurotransmitter GABA in the ventral tegmental area, influencing addictive drug reward behavior (45). Together, these findings suggest that brain-specific LRRC8A deletion disrupts both excitatory and inhibitory signaling, with a broad impact on brain physiology. The significance of VRACs in the brain is underscored by the striking phenotype of mice carrying a brain-wide deletion of LRRC8A in neurons, astrocytes, and oligodendrocytes, using Nestin^{Cre}-driven recombination. Nestin^{Cre+}: LRRC8A$^{-/-}$ mice develop spontaneous seizures and all die between late adolescence and early adulthood (46-48). Our group has linked this lethal phenotype to changes in GABAergic signaling and reactive astrogliosis (47); however, other molecular deficits may also contribute.

The lethal phenotype resulting from LRRC8A deletion in the brain (47) has raised concerns about the therapeutic potential of VRAC blockers and highlighted the need for further investigation into the structure and function of these channels within the CNS. Unlike the essential LRRC8A subunit, the partnering LRRC8 isoforms (LRRC8B–E) are expressed in a cell type-specific manner and modulate the biophysical properties of VRACs, including their permeability to small signaling molecules. The best-established example of this functional diversity is the critical role of LRRC8A and LRRC8D in forming VRACs that preferentially conduct small, uncharged molecules; these include myo-inositol, neutral zwitterions such as taurine, GABA, and glutamine, as well as chemotherapeutic agents like cisplatin and carboplatin (21, 49, 50). Studies in model cell lines suggest that glutamate-permeable VRACs can form through alternative heteromeric assemblies, with LRRC8A pairing separately with LRRC8C, LRRC8D, or LRRC8E or in combination with multiple subunits such as LRRC8C+LRRC8D [see (21, 50, 51) and Discussion]. Despite this extensive body of work, the precise subunit composition and stoichiometry of native VRAC heteromers remain unresolved. To address this knowledge gap, the present study investigated the LRRC8 subunit determinants of endogenous glutamate-permeable VRACs in primary mouse astrocytes, employing both an RNAi approach and genetically modified animals.

MATERIALS AND METHODS

Ethical Approval

All animal procedures used in the present study were approved by the Institutional Animal Care and Use Committee of Albany Medical College (ACUP 24-03002), and strictly conformed to the Guide for the Care and Use of Laboratory Animals as adopted by the U.S. National Institutes of Health (https://grants.nih.gov/grants/olaw/guide-for-the-care-and-use-of-laboratory-animals.pdf).

Animals

This study utilized two types of mice to collect brain tissue and generate primary astrocyte cultures. Wild type (WT) animals were of the C57BL/6J background, originally obtained from the Jackson Laboratory (Farmington, CT, USA; strain #000664, RRID: IMSR_JAX:000664) and bred in-house. Additionally, we used mice with conditional knockout of LRRC8A in the brain (bLRRC8A KO). These were produced by breeding *Lrrc8a*$^{flox/flox}$ females (gift of Dr. Rajan Sah, Washington University School of Medicine, St. Louis, MO, USA) with commercially available *Nestin*$^{Cre/+}$ males (B6.Cg-Tg(Nes-cre)1Kln/J; Jackson Lab stock #003771, RRID:IMSR_JAX:003771). Heterozygous *Nestin*$^{Cre/+}$:*Lrrc8a*$^{flox/+}$ males were further crossed with *Lrrc8a*$^{flox/flox}$ female mice to produce *Nestin*$^{Cre/+}$:*Lrrc8a*$^{flox/flox}$ mice (bLRRC8A KO) and littermate controls. This breeding scheme produces four genotypes, as presented in Fig. 1A. The specificity and efficacy of this genetic strategy were thoroughly validated in our previous work (47, 48). To visualize Cre activity and monitor for unintentional germline recombination, mice were additionally inbred with a strain carrying the Ai9 tdTomato Cre reporter (B6.Cg-Gt(ROSA)26Sor$^{tm9(CAG\text{-}tdTomato)Hze}$/J; Jackson Lab stock #007909, RRID:IMSR_JAX:007909). For simplicity, the presence of the reporter allele is not shown in the breeding diagram. All mice were housed in a temperature, humidity, and light-controlled facility on a 12:12 h light/dark cycle and given free access to food and water.

Brain Tissue Collection and Processing

For brain tissue collection, 14-week-old WT mice were euthanized with a lethal injection of sodium pentobarbital and perfused transcardially, first with room temperature phosphate-buffered saline (PBS), followed by ice-cold PBS. For qRT-PCR analysis, brains were rapidly removed and immediately transferred to a large dissection dish containing ice cold PBS additionally treated with the RNase inhibitor diethyl pyrocarbonate (DEPC, 0.1%). The olfactory bulbs, cerebellum and brainstem were removed, and a midline sagittal cut was made to separate the hemispheres. Each hemisphere was snap-frozen in liquid nitrogen and stored at –80°C until further processing.

Primary Cultures of Mouse Astrocytes

Primary cultures of mouse astrocytes were prepared from brain cortices of newborn (P0-P2) pups of both sexes as most recently described in (48) with minor modifications. Briefly, neonates were anesthetized by cooling and rapidly decapitated. Brains were harvested and

179 transferred into ice-cold sterile Dulbecco's PBS without calcium and magnesium (ThermoFisher
180 Scientific, Waltham, MA, USA, cat. #14190144). Cortical tissue was dissected from meninges,
181 minced using a sterile surgical blade, incubated with 500 µL of the recombinant protease TrypLE
182 Express (ThermoFisher, cat. #12605), and additionally triturated by pipetting. Triturated tissue
183 was digested with TrypLE for 5 min at room temperature (22°C). Enzymatic digestion was
184 terminated by adding Earl's minimal essential medium (MEM, ThermoFisher, cat. #11095)
185 supplemented with 10% heat-inactivated horse serum (HIHS, ThermoFisher, cat. #26050) and
186 penicillin/streptomycin (P/S, ThermoFisher, cat. #15140). The cell suspension was next filtered
187 through a 70-µm nylon mesh cell strainer (Corning, Corning, NY, USA, cat. # 431751). To obtain
188 an enriched astrocyte population, cells extracted from either half brain (for WT), or full brain
189 (bLRRC8A KO) were separately plated onto T75 flasks and grown in a humidified atmosphere of
190 5% CO_2/balance air at 37°C. With this approach, primary cell cultures typically reached confluency
191 after around two weeks and were maintained up to six weeks until replating for functional assays.
192 The purity of astrocyte populations was periodically verified with immunofluorescence by staining
193 for the astrocyte marker, glial fibrillary acidic protein (anti-GFAP, MilliporeSigma, St. Louis, MO,
194 USA, cat. #MAB360, RRID:AB_11212597; 1:400 dilution) and was ≥95%.

195

196 ## Quantitative Real-Time PCR (qRT-PCR)

197 Relative gene expression and efficiency of siRNA gene knockdowns were assessed using
198 qRT-PCR. Total RNA was isolated from brain tissue or primary astrocyte cultures using the Aurum
199 Total RNA Mini Kit (Bio-Rad, Hercules, CA, USA, cat. #732-6820) following the manufacturer's
200 instructions. Processing of tissue samples included on-column DNase digestion to eliminate
201 genomic DNA contamination. RNA concentration was measured with a NanoDrop 1000
202 spectrophotometer (ThermoFisher, RRID:SCR_016517). RNA was immediately converted to
203 cDNA using the iScript cDNA synthesis kit (Bio-Rad, cat. #1708891), with 1 µg of total RNA per
204 20 µL reaction. The resulting cDNA was analyzed for the relative abundance of *Lrrc8* transcripts
205 by qPCR using gene-specific primers and SYBR Green Supermix (Bio-Rad, cat. #1708882) in a
206 CFX96 Real-Time PCR Detection System (Bio-Rad, RRID:SCR_018064). Expression levels were
207 normalized to the housekeeping gene *Rpl13a*, and where applicable, further normalized to control
208 samples using the $2^{-\Delta\Delta C(T)}$ method (52). As an internal quality control, expression of an additional
209 housekeeping gene, *Rps20*, and the abundant transcript *Gapdh* were also quantified. All qPCR
210 primers were obtained as validated GeneGlobe assays from Qiagen (Germantown, MD, USA);
211 detailed catalog information is provided in Table 1.

212

213 ## Western Blotting

214 Relative expression of LRRC8A protein was assessed in lysates from primary astrocyte
215 cultures. Cells were lysed in a denaturing buffer containing 2% sodium dodecyl sulfate (SDS) and
216 8 mM EDTA, followed by dilution with 4× Laemmli sample buffer (Bio-Rad, cat. #4561033).
217 Lysates were boiled for 5 min, and 20 µg of total protein per sample was resolved on 10% Mini-
218 PROTEAN TGX gels (Bio-Rad, cat. #1610747) via SDS-PAGE. Proteins were then transferred to
219 polyvinylidene difluoride (PVDF) membranes (Bio-Rad, cat. #1620177). Membranes were
220 blocked for 20 min in Tris-buffered saline with 0.1% Tween-20 (TBS-T) containing 5% non-fat dry
221 milk and further incubated overnight at 4°C with mouse monoclonal anti-LRRC8A primary

antibody (Santa Cruz, cat. #sc-517113; RRID:AB_2928142; 1:1,000) diluted in the same blocking buffer. After washing in TBS-T, membranes were incubated for 2 h at room temperature with anti-mouse IgG HRP-conjugated secondary antibody (m-IgG Fc BP-HRP, Santa Cruz, cat. #sc-525416; 1:10,000) in 5% milk/TBS-T. Protein bands were visualized using enhanced chemiluminescence reagent (ECL; GE Healthcare, cat. #RPN2232) and a ChemiDoc Imaging System (Bio-Rad, RRID:SCR_019684). For loading controls, membranes were washed and re-probed for 30 min with HRP-conjugated anti-β-actin antibody (Millipore-Sigma, cat. #A3854; RRID:AB_262011; 1:50,000). Band intensities were quantified using ImageJ software (53) (NIH, RRID:SCR_003070). LRRC8A signals were normalized to β-actin immunoluminescence from the same blot.

RNAi-Mediated LRRC8 Gene Silencing

Targeted knockdown of LRRC8 family members was achieved using gene-specific siRNA constructs obtained from Qiagen (Valencia, CA, USA). AllStars Negative Control siRNA (Qiagen) was used as a non-targeting control. Primary astrocytes at ~70–80% confluency were transfected using Lipofectamine RNAiMAX (Thermo Fisher, cat. #13778075) according to the manufacturer's protocol. siRNA-Lipofectamine complexes were prepared in Opti-MEM (Thermo Fisher, cat. #31985), further diluted with Opti-MEM, and added to cells at final siRNA concentrations ranging from 10 to 50 nM (optimized for individual siRNAs). Details of the siRNA constructs, including catalog numbers and target sequences, are listed in Table 1. Knockdown efficiency for each construct was validated by qRT-PCR. After a 4 h incubation, cultures were supplemented with MEM containing 10% HIHS and penicillin plus streptomycin (MEM+HIHS+P/S). At 24 h post-transfection, the medium was fully replaced with fresh MEM+HIHS+P/S. mRNA expression levels were assessed 48 h post-transfection, and functional assays were performed 96 h post-transfection.

Radiotracer Assays of VRAC Activity

VRAC activity was evaluated by measuring the release of D-[^{3}H]aspartate, a non-metabolizable analog of glutamate, as extensively validated in our earlier studies [e.g., (50, 54, 55)]. Two complementary assay formats were used, employing astrocytes cultured either in multi-well plates or on glass coverslips. In all experiments, astrocytes were preloaded overnight in standard serum-containing medium supplemented with 2 μCi/mL D-[^{3}H]aspartate (Revvity, cat. #NET50100).

For medium-throughput screening of multiple siRNA constructs, cells were grown on poly-D-lysine-coated 12-well plates. After radiotracer loading, cultures were washed to remove extracellular isotope and equilibrated for 30 min at 37°C in isoosmotic Basal medium containing (in mM): 135 NaCl, 3.8 KCl, 1.2 $MgSO_4$, 1.3 $CaCl_2$, 1.2 KH_2PO_4, 10 D-glucose, and 10 HEPES (pH 7.4; osmolality 290 ±3 mOsm/kg). To inhibit radiotracer reuptake via the Na^+-dependent GLAST transporters, cells were exposed to LiCl-substituted media, in which NaCl was isoosmotically replaced with LiCl (56). Baseline release was measured during a 10-min incubation in isoosmotic Li^+-containing medium, followed by stimulation with hypoosmotic Li^+ medium (LiCl reduced by 50 mM; final osmolality ~200 mOsm/kg, ~30% reduction) to activate VRAC. Ten-min fractions of isoosmotic and hypoosmotic media were collected for analysis. Radiotracer release was quantified by liquid scintillation counting using a TRI-CARB 4910TR counter (Revvity), after

265 mixing samples with Ecoscint A scintillation fluid (National Diagnostics, cat. #LS-273). Integral
266 release values were normalized to the remaining intracellular D-[^{3}H]aspartate, determined after
267 cell lysis in 2% SDS containing 8 mM EDTA.
268 To resolve the kinetics of VRAC activation, D-[^{3}H]aspartate efflux assays were conducted
269 using a custom-fabricated Lucite superfusion chamber that has a depression on the bottom to
270 accommodate an 18 × 18 mm glass coverslip and a Teflon screw lid that leaves a ~200 µm space
271 above the cells. Coverslips with D-[^{3}H]aspartate-preloaded astrocytes were briefly washed with
272 Basal medium (for composition see above), transferred into the chamber, and superfused at a
273 constant rate of ~1.4 mL/min with either isoosmotic or hypoosmotic media. In this setup, we used
274 NaCl-containing media because released D-[^{3}H]aspartate was effectively removed with the flow.
275 One-min perfusate fractions were collected into scintillation vials using an automated CF-1
276 fraction collector (SpectraLab Scientific, Markham, ON, Canada). At the conclusion of each
277 experiment, cells were lysed in 2% SDS+8 mM EDTA, and D-[^{3}H]aspartate content in all samples
278 was quantified using a scintillation counter as described above. Data were expressed as fractional
279 release values, calculated at each time point as a ratio of released [^{3}H] to the total [^{3}H] content
280 (cumulative release + remaining tracer), using a custom Excel-based analysis program.
281
282 ### Statistics

283 All data are presented as mean values ± SD. n value corresponds to an individual animal (qPCR
284 and RNA-seq) or an independently transfected astrocyte culture. For cell culture experiments, all
285 results were reproduced in multiple cultures prepared from at least two different animals, unless
286 specified otherwise. Statistical differences between three or more groups were analyzed using
287 one-way ANOVA followed by Tukey's multiple comparisons test. For functional assays conducted
288 in a multi-well plate format, statistical differences were examined using repeated measures two-
289 way ANOVA assessing the effects of medium (cell swelling), treatment (siRNA), and their
290 interaction, followed by Tukey's multiple comparisons test. For clarity, we present only the effects
291 of treatment, but full analyses are included in the primary datasets deposited in the Open Science
292 Framework (osf.io). In RNAi expression assays, mRNA expression values were normalized to the
293 expression levels in siNC-treated cells and compared to a unity using one-sample t-test with
294 Bonferroni correction for multiple testing (adjusted p = p × number of comparisons). All statistical
295 analyses and graph preparation were performed using GraphPad Prism 10.0 (GraphPad
296 Software, San Diego, CA, USA; RRID:SCR_002798).
297

298 # RESULTS

299

300 ### LRRC8A Deletion Abolishes Activity of Glutamate-Permeable VRACs in Astrocytes

301 To investigate the role of LRRC8 proteins in the formation of endogenous astrocytic
302 VRACs, we first employed a molecular genetics approach using *Nestin*^{Cre}-driven recombination.
303 *Nestin*^{Cre} targets neural precursor cells, leading to gene deletion in all cells of neuroectodermal
304 origin, including astrocytes (57, 58). Our conditional knockout breeding strategy produced four
305 genotypes: two types of controls (*Lrrc8a*$^{flox/+}$ and *Lrrc8a*$^{flox/flox}$ without Cre, referred to as fl/+ and
306 fl/fl), a heterozygous (HET) LRRC8A deletion, and a homozygous LRRC8A knockout (KO) (Fig.
307 1A1). Primary astrocyte cultures were prepared from neonatal brains of each genotype and
308 successful Cre recombination was confirmed using the Ai9 tdTomato reporter. Live-cell imaging
309 of tdTomato fluorescence showed complete Cre penetrance in both LRRC8A HET and KO

310 astrocytes (representative image in Fig. 1A2). Western blot analysis of astrocyte culture lysates
311 revealed that heterozygous LRRC8A deletion reduced LRRC8A protein levels by approximately
312 60% ($p < 0.0001$, Fig. 1B), while KO cultures showed a complete loss of LRRC8A
313 immunoreactivity ($p < 0.0001$, Fig. 1B, full western blot dataset in Supplemental Fig. 1).

314 *Insert Fig. 1 near here*

315 We next assessed functional VRAC activity using a D-[^{3}H]aspartate efflux assay. In control
316 astrocytes, a 30% reduction in extracellular osmolality (to 200 mOsm) triggered a rapid increase
317 in D-[^{3}H]aspartate release, reaching a peak rate of 2.6% within two minutes (an 8.7-fold rise over
318 baseline) followed by a gradual decline consistent with the volume regulatory process. This kinetic
319 profile closely matched our previous measurements of VRAC activation in both rat and mouse
320 astrocytes (50, 54). Astrocytes with heterozygous LRRC8A deletion exhibited a 30% reduction in
321 swelling-activated radiotracer efflux ($p = 0.038$, Fig. 1C, full analysis in Supplemental Fig. 2). As
322 anticipated, LRRC8A KO astrocytes displayed a profound loss of swelling-induced glutamate
323 release ($p < 0.0001$, Fig. 1C and Supplemental Fig. 2). However, a small, transient release
324 component persisted during the initial three minutes of hypoosmotic exposure (Fig. 1C). This
325 residual response was characterized by more rapid activation and inactivation kinetics as
326 compared to typical VRAC-mediated release and is likely mediated by a distinct mechanism (see
327 additional considerations in the following paragraph and extended Discussion). Notably, LRRC8A
328 KO astrocytes also showed a substantial reduction in baseline glutamate release under
329 isoosmotic conditions: 28% lower than that of littermate controls ($p < 0.0001$ see inset in Fig. 1C).
330 Together, these findings demonstrate that (i) LRRC8A containing VRACs are the primary conduit
331 for swelling-induced glutamate release in astrocytes, and (ii) these channels also contribute to
332 tonic glutamate release under resting, isoosmotic conditions.

333 To further investigate the apparent discrepancy between the 60% decrease in LRRC8A
334 protein levels and the relatively modest 30% inhibition of swelling-activated glutamate release in
335 HET cells, we performed additional functional assays using media with a more pronounced
336 reduction in osmolality. When medium osmolality was decreased by ~50% (to 150 mOsm), VRAC
337 activation was dramatically enhanced compared to the response observed with a 30% (to
338 200mOsm) osmotic reduction, resulting in an over 10-fold increase in maximal release rates
339 between the two conditions (compare Y-axis scales in Fig. 1C and 1D). LRRC8A KO cells again
340 showed a significant reduction in baseline glutamate release, a 40% decrease as compared to
341 controls ($p < 0.0001$, Fig. 1D, consistent with Fig. 1C). Importantly, in severely swollen astrocytes,
342 heterozygous LRRC8A deletion caused a much more pronounced 62% reduction in VRAC-
343 mediated activity, which is close to what would be expected based on changes in protein
344 expression in HET cells ($p < 0.0001$, Fig. 1D, full analysis in Supplemental Fig. 3). These results
345 may suggest that a reserve pool of LRRC8A-containing anion channels in the HET genotype can
346 compensate under moderate swelling conditions, but this compensatory capacity is lost with more
347 extreme osmotic stress/cellular swelling (see Discussion). This finding has implications for
348 interpreting subsequent RNAi-based knockdown experiments.

349 Finally, an important observation was made while comparing the "residual" D-[^{3}H]aspartate
350 release in LRRC8A KO astrocytes exposed to 30% and 50% reductions in medium osmolality. In
351 LRRC8A KO cells, the magnitude of this residual release was indistinguishable between the two
352 hypoosmotic conditions (the maximal release rates: 0.62 ± 0.25% vs. 0.51 ± 0.32%, $p = 0.4975$,
353 insets in Fig. 1C and 1D). This was in striking contrast to control astrocytes, where VRAC activity
354 increased by an order of magnitude under stronger osmotic stress (2.59 ± 0.55% vs. 26.38 ±
355 5.19%, $p < 0.0001$). This lack of sensitivity to the extent of cellular swelling further supports the
356 conclusion that the residual release observed in LRRC8A KO astrocytes is not mediated by VRAC
357 (see Discussion).

358

359 ## Relative Abundance of *Lrrc8* Transcripts in Mouse Brain and Primary Astrocyte Cultures

360 We next measured and compared the endogenous expression of all five *Lrrc8* isoforms in
361 C57BL/6J mouse brains and primary astrocyte cultures derived from C57BL/6J neonates. qPCR
362 analysis of samples prepared from forebrain tissue detected high levels of four *Lrrc8* transcripts,
363 *Lrrc8a-Lrrc8d*, with the order of abundance *Lrrc8b>Lrrc8a≈Lrrc8d>Lrrc8c* (Fig. 2A). mRNA levels
364 of the *Lrrc8* subunits were ~1–5% of the housekeeping gene ribosomal *Rpl13a*, or 0.5–2.5% of
365 the highly prevalent *Gapdh* (Fig. 2A and Supplemental Fig. 4A). Consistent with literature reports,
366 brain levels of *Lrrc8e* were very low-to-non-detectable (Fig. 2A). To independently validate our
367 findings on *Lrrc8* expression, we additionally performed an in-silico analysis of publicly available
368 RNAseq datasets. Figure 2B summarizes expression levels of the five *Lrrc8* isoforms in seven
369 forebrain regions from five mice of both sexes from the Human Protein Atlas. The pattern of
370 relative abundance of *Lrrc8* subunits in RNAseq datasets was nearly identical to those found in
371 our qRT-PCR experiments: *Lrrc8b>Lrrc8d≈Lrrc8a>Lrrc8c*, and extremely low-to-nondetectable
372 *Lrrc8e* (compare Fig. 2A and 2B). Transcripts Per Million (TPM) values of ≥10 confirmed that
373 *Lrrc8a-d* transcripts are highly abundant in the mouse brain.

374 *Insert Fig. 2 near here*

375 In primary astrocyte cultures, the average levels of *Lrrc8* transcripts were comparable to
376 those observed in forebrain tissue. Expression levels of the four predominant *Lrrc8* isoforms
377 ranged from ~1–4% relative to *Rpl13a*, or 0.5–2% when normalized to *Gapdh* (Fig. 2C and
378 Supplemental Fig. 4B). As in brain tissue, *Lrrc8e* expression was detected at trace levels (Fig.
379 2C). Notably, we observed cell type-specific differences in the relative expression of individual
380 *Lrrc8* isoforms: cultured astrocytes exhibited significantly higher levels of *Lrrc8c* and markedly
381 lower levels of *Lrrc8b* compared to brain tissue (compare Fig. 2A and Fig. 2C). These differences
382 may reflect an intrinsic cell type-specific *Lrrc8* expression profile or could result from artifacts
383 introduced by *in vitro* culture conditions.

384

385 ## Analysis of Subunit-Specific Contributions of LRRC8B-E to Glutamate-Permeable VRACs

386 To assess the individual contributions of the five LRRC8 isoforms to glutamate
387 permeability, we employed an RNA interference (RNAi) approach using commercially available
388 siRNA constructs. For each of the five *Lrrc8* mRNA species, we tested three distinct siRNA
389 constructs targeting different regions of the mRNA (see Table 1 for target sequences). In cells
390 treated with a non-targeting control siRNA (siNC) the relative expression profile remained
391 unchanged (compare Fig. 2C and Fig. 3A1). All tested siRNA constructs achieved 70–90%
392 knockdown of their respective targets (Fig. 3B1–F1). Therefore, all siRNA constructs were
393 included in the initial functional screenings.

394 *Insert Fig. 3 near here*

395 To increase experimental throughput, initial VRAC activity assays were conducted in a
396 multi-well plate format, measuring swelling-activated D-[^{3}H]aspartate release in response to a
397 30% reduction in medium osmolarity (see schematic Fig. 3A2). As detailed in the Methods
398 section, these efflux assays were performed in Na^+-free medium to prevent reuptake of the tracer
399 by Na^+-dependent GLAST transporters. For all experiments, repeated measures two-way ANOVA
400 revealed a main effect of medium osmolarity (basal vs. hypoosmotic, $p<0.0001$), consistent with
401 activation of VRACs (Fig. 3B2-F2). For simplicity, we present only the post-hoc analyses
402 comparing the effects of individual siRNA constructs to siNC-treated controls under hypoosmotic
403 conditions. We first tested the effect of siRNA-mediated knockdown of the essential LRRC8A

404 subunit. All three siRNAs targeting LRRC8A (designated siA1, siA3, and siA4) strongly reduced
405 swelling-induced D-[^{3}H]aspartate release, decreasing it by 67–85% as compared to siNC controls
406 ($p < 0.0001$ vs. siNC; Fig. 3B2). The degree of inhibition ranked siA1 > siA3 > siA4 (Fig. 3B2).
407 Importantly, the high inhibitory potency of the LRRC8A knockdown resembled the near-complete
408 loss of VRAC activity in LRRC8A KO astrocytes.

409 In contrast to the potent effect of LRRC8A knockdown, none of the siRNAs targeting
410 LRRC8B (siB1, siB3, and siB4) inhibited VRAC activity (Fig. 3C2). However, repeated measures
411 two-way ANOVA revealed a significant interaction between siRNA treatments and media
412 osmolarity ($p=0.02$; Fig. 3C2), so we performed a post hoc analysis. Interestingly, one construct,
413 siB1, produced a statistically significant 24% increase in swelling-activated D-[^{3}H]aspartate
414 release ($p = 0.002$ vs. siNC; Fig. 3C2). For all subsequent experiments, we used siB4, which
415 demonstrated high efficacy in reducing *Lrrc8b* mRNA levels, while not affecting functional VRAC
416 activity.

417 All three siRNA constructs targeting LRRC8C (siC1, siC2, and siC4) significantly reduced
418 VRAC activity ($p <0.0001$ vs. siNC; Fig. 3D2). The most effective, siC1, reduced swelling-
419 activated D-[^{3}H]aspartate release by 56% ($p <0.0001$ vs. siNC; Fig. 3D2). The order of inhibition
420 was siC1 > siC4 > siC2, which closely mirrored the efficacy of *Lrrc8c* mRNA knockdown (Fig.
421 3D1). Due to its superior efficacy, siC1 was used in all subsequent functional assays. The
422 prominent contribution of LRRC8C to VRAC-mediated glutamate release in mouse astrocytes
423 was surprising and contrasted with previous reports in other cell types, including our own findings
424 in rat astrocytes, which showed that LRRC8C knockdown does not meaningfully impact swelling-
425 activated D-[^{3}H]aspartate efflux (see (50) and Discussion).

426 LRRC8D knockdowns produced more nuanced effects. Two of the tested siRNA
427 constructs, siD2 and siD4, reduced VRAC activity by 10% and 28%, respectively ($p = 0.542$ and
428 0.002 vs. siNC, Fig. 3E2). In contrast, siD1 produced a striking 60% increase in swelling-activated
429 D-[^{3}H]aspartate release ($p <0.0001$ vs. siNC; Fig. 3E2). Follow-up qRT-PCR analysis revealed
430 that siD1 induced off-target effects, leading to a paradoxical upregulation of *Lrrc8a* and *Lrrc8c*
431 transcript levels by 2.5-fold and 1.7-fold, respectively (Supplemental Fig. 5). Based on its superior
432 efficacy and lack of off target-effects, siD4 was used in all subsequent experiments. Overall, these
433 findings suggest that LRRC8D plays a role in glutamate-permeable VRAC function, though its
434 contribution is relatively limited.

435 Finally, we tested three siRNA constructs targeting LRRC8E (siE1, siE2, and siE4).
436 Although the LRRC8E subunit is expressed in mouse astrocytes at only trace levels (see Fig. 2C),
437 our prior work in rat astroglia has suggested that LRRC8E may be incorporated into astrocytic
438 VRAC and modulate swelling-activated glutamate release (50). In the current study, LRRC8E
439 knockdown had no biologically significant effect on VRAC activity in mouse astrocytes, albeit
440 small increases in VRAC activity were observed with all siRNA constructs ($p = 0.001$ vs. siNC,
441 Fig. 3F2).

442

443 **Non-Redundant Functions of LRRC8C and LRRC8D in Glutamate-Permeable VRACs**

444 While LRRC8C knockdown strongly suppressed swelling-activated D-[^{3}H]aspartate
445 release (Fig. 3D2), the resulting inhibition was less pronounced than that observed with knock-
446 down of the essential LRRC8A subunit (compared to Fig. 3B2). These findings suggest that other
447 LRRC8 proteins may function redundantly with LRRC8C in forming heteromeric VRACs. This
448 hypothesis aligns with the original discovery that individual LRRC8B–E subunits are dispensable
449 for VRAC function in HEK293 and other cells (32, 33). It is also consistent with our earlier work
450 showing that, in rat astrocytes, LRRC8C and LRRC8D serve as mutually replaceable partners of

451 LRRC8A in forming glutamate-permeable VRACs (50). To test if this redundancy extends to
452 mouse astrocytes, we performed a double-knockdown of LRRC8C and LRRC8D.

453 We first verified that co-transfection with siRNAs targeting *Lrrc8c* (siC1) and *Lrrc8d* (siD4)
454 effectively reduced target gene expression by ≥80%, both individually and in combination ($p<0.01$,
455 $p<0.05$; Fig. 4A). Functional assays performed in a multi-well plate revealed that dual knockdown
456 of LRRC8C and LRRC8D did not further decrease glutamate release as compared to LRRC8C
457 knockdown alone (60% vs. 56% inhibition, $p = 0.240$, Fig. 4B). To assess VRAC activity with
458 higher temporal resolution, we repeated the double-knockdown experiments using a Lucite
459 superfusion system. In this setup, LRRC8C knockdown reduced the maximum rate of glutamate
460 release by 33%, while LRRC8C+D knockdown lowered it by 44%; however, this difference was
461 not statistically significant ($p = 0.7591$; Fig. 4C). Analysis of the integral VRAC-mediated release
462 under hypoosmotic conditions showed a small difference between siC1 alone and the siC1+siD4
463 combination ($p = 0.011$, Supplemental Fig. 6A). While differences in the degree of VRAC inhibition
464 between plate-based and superfusion assay formats were noted, the lack of additive effect
465 between LRRC8C and LRRC8D knockdowns was consistent across both.

466 *Insert Fig. 4 near here*

467 Our LRRC8A KO data, particularly the results of the heterozygous LRRC8A deletion,
468 suggest that in cells exposed to a 30% reduction in medium osmolality, VRAC channels may have
469 a spared capacity obscuring the full effects of LRRC8 subunit knockdown. Therefore, we repeated
470 the double-knockdown experiments in astrocytes exposed to a 50% reduction in medium
471 osmolarity (Fig. 4D). Under these conditions, knockdowns of individual LRRC8C and LRRC8D
472 subunits strongly inhibited VRAC activity (50% and 42% decrease in maximal release rates,
473 respectively; $p<0.0001$ vs. siNC, Fig. 4D, additional analysis in Supplemental Fig. 6B). The double
474 knockdown of LRRC8C plus LRRC8D produced partially additive inhibition as compared to single
475 knockdowns (a 72% decrease, $p=0.004$, vs LRRC8C and $p =0.0001$ vs. LRRC8D alone, Fig. 4D
476 and Supplemental Fig. 6B). Partial additivity of the double-knockdown (as opposed to synergistic
477 effect) is consistent with the existence of separate LRRC8A+LRRC8C and LRRC8A+LRRC8D-
478 containing heteromeric VRACs (see Discussion).

479

480 **Functional Contribution of LRRC8B to LRRC8C- and LRRC8D-Containing VRACs**

481 Given that the combined downregulation of LRRC8C and LRRC8D did not reach the full
482 effect of LRRC8A knockdown, we hypothesized that another abundant LRRC8 isoform, namely
483 LRRC8B, serves as a functional substitute for either LRRC8C and/or LRRC8D. To test this
484 hypothesis, we explored the potential contribution of LRRC8B in double-knockdown siRNA
485 assays. We predicted that knocking down either LRRC8C+LRRC8B or LRRC8D+LRRC8B would
486 produce a more substantial functional effect than knocking down of LRRC8C or LRRC8D alone.

487 We first tested the efficacy of the double-knockdown of LRRC8B and LRRC8C. qRT-PCR
488 analysis confirmed that siB4 and siC1 constructs were equally effective when transfected alone
489 or in combination ($p<0.01$, $p<0.05$; Fig. 5A). Unexpectedly, in VRAC activity assays, the double
490 knockdown of LRRC8B and LRRC8C resulted in a partial rescue of VRAC-mediated glutamate
491 release as compared to the effect of LRRC8C knockdown on its own ($p<0.0001$ vs. siNC; Fig.
492 5B). Specifically, the siB4 construct had no effect ($p= 0.98$; Fig. 5B), siC1 suppressed VRAC
493 activity by 51% ($p<0.0001$; Fig. 5B), and the combination of siB4 and siC1 paradoxically caused
494 a smaller 25% inhibition ($p < 0.0001$, siB1+C1 vs. siC1 alone, Fig. 5B).

495 *Insert Fig. 5 near here*

496 In a similar fashion, we quantified the efficacy of the double-knockdown of LRRC8B and
497 LRRC8D. qRT-PCR analysis verified that siB4 and siD4 constructs were equally effective when
498 transfected alone or in combination ($p<0.001$; Fig. 5C). In functional assays, the double
499 knockdown of LRRC8B and LRRC8D resulted in a complete rescue of the VRAC-mediated
500 glutamate release as compared to the effect LRRC8D knockdown on its own (Fig. 5D).
501 Specifically, siB4 had no effect ($p= 0.4145$; Fig. 5D), siD4 reduced VRAC activity by 17%
502 ($p<0.001$; Fig. 5D), and the combination of siB4 and siD4 caused full recovery of glutamate
503 release in hypoosmotic medium (Fig. 5D).

504 It important to note that the rescue effects of co-transfection with siB4 were subunit
505 specific. In experiments involving the combined knockdown of LRRC8A+LRRC8B, the effect of
506 siA1+siB4 was no different from the effect of siA1alone (Supplemental Fig. 7A). Overall, these
507 data suggest that LRRC8B can act as a structural partner in LRRC8A+LRRC8C and
508 LRRC8A+LRRC8D containing channels.

509

DISCUSSION

The main objective of this study was to identify which LRRC8 isoforms contribute to the formation of glutamate-permeable VRACs in mouse astrocytes. VRAC activation in this cell type is considered a major source of pathological glutamate release and a possible therapeutic target in stroke and other CNS disorders [see ref. (44) and reviews (17, 18, 23)]. Our key findings can be summarized as follows: (1) Genetic knockout of the essential LRRC8A subunit confirms that LRRC8A-containing VRACs are the primary pathway for swelling-activated glutamate release in moderately swollen astrocytes and account for ~98% of the release under conditions of substantial cell swelling. (2) Results of siRNA-mediated knockdown of LRRC8A through LRRC8E, individually and in combination, support a model in which glutamate-permeable VRACs critically depend on LRRC8A and LRRC8C, with likely structural contribution from LRRC8B. (3) The LRRC8D subunit provides an additional contribution to swelling-activated glutamate release but is likely present in a distinct subpopulation of VRACs.

Despite extensive work in the field, there is ongoing debate over whether VRACs represent the primary pathway for swelling-activated glutamate release, particularly in astrocytes. Several studies have proposed alternative molecular candidates as major, or even primary, conduits for swelling- and/or Ca^{2+}-activated glutamate release from astrocytes, including SLCO2A1-containing Maxi Cl^- channels (59, 60), Ca^{2+}-activated BEST1 channels (61, 62), and channels formed by the Tweety homolog proteins TTYH1–3 (63). Furthermore, astroglial Cx43 hemichannels (64) and the $P2X_7$ receptor-activated pannexin complexes (65, 66) may also release amino acid transmitters in response to various stimuli. Our current findings in genetically modified astrocytes show that deletion of the essential LRRC8A subunit virtually abolishes swelling-activated glutamate release. Consistent with our earlier study (47), we observed a small residual release in LRRC8A KO astrocytes, which was insensitive to the extent of cell swelling. We speculate that this residual release in LRRC8A KO cells is mediated by one of the above-mentioned alternative permeability routes, which may be activated by Ca^{2+}. Although the molecular nature of this additional release component is not clear, it is cell volume independent, and its quantitative contribution is minimal. Interestingly, as compared to cells prepared from littermate controls, LRRC8A KO astrocytes display a significant reduction in tonic glutamate release under isoosmotic conditions. Overall, this part of our work suggests that (1) LRRC8A-containing VRACs dominate the swelling-activated release of cytosolic excitatory amino acids, and (2) VRACs exhibit limited tonic activity in non-swollen cells.

While the *Lrrc8a* gene product can be found in virtually all vertebrate cells, the mRNA and protein expression profiles of partnering *Lrrc8* subunits exhibit cell type-, tissue-, and species-specific differences (34, 67). For example, a recent comprehensive study in the mouse cochlea revealed that in this organ different cell types can express dramatically different assortments of LRRC8 proteins (68). Therefore, we first explored and compared the *Lrrc8* transcript profiles in mouse brain tissue and primary mouse astrocytes. qRT-PCR analysis of the mouse forebrain revealed abundant expression of *Lrrc8a* through *Lrrc8d* mRNA, while *Lrrc8e* levels were low to undetectable. These results were corroborated by an *in-silico* analysis of publicly available RNA-seq datasets. Interestingly, both approaches revealed particularly high brain expression of *Lrrc8b*. The relevance of this finding is not clear given that the LRRC8B protein is yet to be reliably associated with any established VRAC function. In mouse astrocyte cultures, qRT-PCR revealed generally similar *Lrrc8* expression patterns. However, we noted a shift in the relative abundance

555 of specific subunits: *Lrrc8c* was expressed at ~3-fold higher levels, while *Lrrc8b* expression was
556 reduced ~3.5-fold compared to the forebrain. Whether these differences reflect a cell type-specific
557 expression profile or adaptations to *in vitro* culture conditions remains to be determined. Notably,
558 our analyses also revealed species-specific differences in *Lrrc8* transcript levels. In the human
559 brain, *Lrrc8a* dominates over other *Lrrc8b-d* isoforms with *Lrrc8e* being largely absent (see RNA-
560 seq data in a Supplemental Fig. 8). In rat brain and astrocytes, *Lrrc8a* through *Lrrc8d* are detected
561 in similar quantities, whereas astrocytic *Lrrc8e* is expressed at low but functionally relevant levels
562 (50). These species-dependent expression patterns are important to consider when interpreting
563 functional data presented in this study.

564 Our understanding of the subunit composition of VRACs capable of conducting organic
565 anions, including the neurotransmitters glutamate and aspartate, remains incomplete and
566 somewhat contradictory. In CRISPR/Cas9-edited HEK293 cells, only LRRC8A+LRRC8D and
567 LRRC8A+LRRC8E heteromers show significant conductance of the glutamate analog D-[^{3}H]as-
568 partate, while LRRC8A+LRRC8C channels showed little activity (21). In comparison, the results
569 of heterologous expression in *Xenopus* oocytes demonstrated that LRRC8A+LRRC8C and
570 LRRC8A+LRRC8E channels exhibit measurable glutamate permeability (51). The latter *Xenopus*
571 study also reported glutamate release through LRRC8A+LRRC8D heteromers, albeit at lower
572 rates (51). Our own RNAi analysis in rat astrocytes indicated that endogenous glutamate-
573 permeable VRACs are composed of LRRC8A, LRRC8C, and LRRC8D proteins, with a possible
574 minor contribution from LRRC8E (50). In support of this complex heteromeric assembly, work in
575 model cell lines, such as HEK and HeLa cells, has shown that individual deletion of LRRC8B
576 through LRRC8E does not lead to an appreciable reduction of VRAC activity, suggesting that
577 these subunits play interchangeable roles in channel function (33, 35). Given this background, we
578 were surprised to find that in mouse astrocytes, swelling-activated glutamate release was strongly
579 dependent on the expression of LRRC8C (56% inhibition observed following LRRC8C knock-
580 down). To our knowledge, the only comparable recent finding is the complete loss of VRAC
581 currents and swelling-activated cyclic dinucleotide transport in mouse T lymphocytes after genetic
582 deletion of LRRC8C (69). Taken together, these data suggest that in mouse astrocytes,
583 endogenous VRACs are predominantly formed by LRRC8A and LRRC8C, with limited functional
584 input from other LRRC8 subunits.

585 In rat astrocytes, glutamate-permeable VRACs are formed with redundant contributions
586 of LRRC8C and LRRC8D (50). In this species, knockdown of either LRRC8C or LRRC8D alone
587 had no significant effect, whereas combined knockdown of both subunits caused strong inhibition
588 of swelling-activated D-[^{3}H]aspartate release (50). Based on this observation, we tested the effect
589 of combined LRRC8C and LRRC8D knockdown in mouse astroglia. Surprisingly, in mouse
590 astrocytes subjected to moderate hypotonic stress (30% reduction in medium osmolality), a
591 combination of siRNAs targeting LRRC8C and LRRC8D produced no additional inhibition beyond
592 that seen with LRRC8C knockdown alone. This result was confirmed using two independent
593 assay systems. However, when cells were exposed to more severe hypotonic stress (50%
594 reduction in medium osmolality), LRRC8D knockdown alone exerted a stronger inhibitory effect
595 on glutamate release, and the combined knockdown of LRRC8C and LRRC8D produced partially
596 additive effects. The lack of synergy between LRRC8C and LRRC8D knockdown in mouse
597 astrocytes is consistent with a model in which LRRC8C and LRRC8D contribute to distinct
598 populations of VRACs (see Fig. 6). Previously, we and others have shown that LRRC8A+
599 LRRC8D heteromers form a specific VRAC subtype that preferentially conducts uncharged and
600 net-neutral osmolytes, such as taurine, GABA, and myo-inositol, but also exhibits measurable

601 permeability to glutamate (21, 49, 50). The current data support the existence of two separate
602 channel populations (LRRC8A+LRRC8C) and (LRRC8A+LRRC8D) with distinct permeability
603 profiles.

604 *Insert Fig. 6 near here*

605 Finally, we would like to discuss potential contributions of LRRC8B. Although highly
606 expressed in the brain [ref. (34) and current data], this subunit does not yet have an established
607 physiological role. Even though LRRC8B is present in endogenous VRACs, heteroexpression of
608 LRRC8A+LRRC8B in model cell lines or their reconstitution in lipid bilayers does not produce
609 functional VRAC currents (21, 33, 35, 51). Among the five LRRC8 isoforms, only LRRC8A and
610 LRRC8B contain charged arginines in the narrowest part of the channel (R103 and R99, respect-
611 tively) (36-38). In contrast, LRRC8C-E contain neutral leucine or phenylalanine in the same
612 position, and the presence of these subunits results in a wider VRAC pore (70). The only reported
613 physiological role of LRRC8B is the increased Ca^{2+} leak from the endoplasmic reticulum in
614 HEK293 cells overexpressing LRRC8B, and reciprocally, slower depletion of ER calcium stores
615 caused by LRRC8B knockdown (71). Our current data show that in mouse astrocytes, individual
616 LRRC8B knockdowns did not produce inhibition of glutamate-permeable VRACs (one of three
617 effective siRNAs weakly *stimulated* VRAC activity). However, when LRRC8B was downregulated
618 in combination with LRRC8C or LRRC8D, it partially rescued the inhibitory effects of targeting
619 LRRC8C or LRRC8D subunits alone. Interestingly, in the CRISPR/ Cas9-edited HEK293 cells,
620 LRRC8B deletion also caused a noticeable increase in swelling-activated D-[^{3}H]aspartate efflux
621 (21). Together, these findings suggest that LRRC8B is present in glutamate-permeable VRACs
622 but paradoxically restricts their permeability for this amino acid. We speculate that LRRC8B can
623 structurally substitute for downregulated LRRC8C or LRRC8D in the heteromeric VRACs.
624 However, the resulting LRRC8B "enrichment" may make the VRAC pore narrower, much like what
625 has been reported for the homomeric LRRC8A assemblies (36, 37, 39).

626 In summary, this study provides important insights into the subunit composition of native
627 glutamate-permeable VRACs in the mouse brain and may serve as a steppingstone for the
628 development of subunit-specific VRAC blockers. Beyond their many physiological roles, VRACs
629 are recognized as significant contributors to glutamate-driven tissue damage in stroke, traumatic
630 brain injury, and possibly epilepsy (17, 22, 23). Adding to VRACs' clinical relevance, a recent
631 study discovered that gain-of-function mutations in the human *LRRC8C* gene cause a multi-
632 system disorder named TIMES [Telangiectasia, Impaired intellectual development, Microcephaly,
633 Eye abnormalities, and Short stature (72)]. These mutations lead to constitutive VRAC activity
634 and are associated with severe neurological deficits including an abnormally small brain, optic
635 nerve atrophy, spasticity, and seizures (72). Targeting glutamate-permeable VRACs may mitigate
636 hyperexcitability and neurotoxicity in CNS disorders, with more limited impact on broader VRAC
637 functions in other organs and tissues.

638 # DATA AVAILABILITY

639 All primary data included in this manuscript have been archived in the Open Science Framework
640 depository (osf.io) and can be accessed at https://osf.io/cdxqf

641

642 # SUPPLEMENTAL MATERIAL

643 The following supplemental figures for the manuscript are referred to in the text and can be found
644 at https://osf.io/cdxqf or at https://doi.org/10.6084/m9.figshare.29636810

645 **Supplemental Figure 1**. Full-length western blots of LRRC8A and β-actin immunoreactivity in
646 four sets of astrocyte culture lysates derived from LRRC8A fl/+, fl/fl, HET, and KO neonates.

647 **Supplemental Figure 2**. Extended statistical analysis of swelling-activated D-[^{3}H]aspartate
648 release from genetically modified astrocytes in response to a 30% reduction in medium
649 osmolarity.

650 **Supplemental Figure 3**. Extended statistical analysis of swelling-activated D-[^{3}H]aspartate
651 release from genetically modified astrocytes in response to a 50% reduction in medium
652 osmolarity.

653 **Supplemental Figure 4**. Additional qRT-PCR analysis and Ct values of *Lrrc8a-e* expression in
654 mouse forebrain (A) and primary astrocyte cultures (B).

655 **Supplemental Figure 5**. qRT-PCR analysis of all five *Lrrc8* transcripts in primary mouse
656 astrocytes treated with three independent *Lrrc8d* gene-specific siRNA constructs (siD1, siD2,
657 siD4).

658 **Supplemental Figure 6**. Extended statistical analysis of VRAC activity in mouse astrocytes
659 treated with siNC, siC1, siD4, or siC1+siD4 in response to a 30% or 50% reduction in medium
660 osmolarity.

661 **Supplemental Figure 7**. Additivity experiments assessing the combinatory effect of double
662 LRRC8A+B knockdown or LRRC8C+E knockdown on swelling-activated D-[^{3}H]aspartate release
663 from mouse astrocytes.

664 **Supplemental Figure 8**. RNA-seq analysis of *LRRC8A-E* expression in four human brain regions
665 (cortex, amygdala, caudate, and hippocampus)

666

667 # ACKNOWLEDGMENTS

668 The authors thank Dr. Preeti Dohare for help with validating LRRC8D siRNA constructs and
669 Antonio M. Fidaleo for his assistance in RNA-seq analyses.

670

GRANTS

This study was supported by the National Institutes of Health, grants R01 NS111943 and R21 NS140782 (to A.A.M.).

DISCLOSURES

The authors have no conflict of interest, financial or otherwise, to disclose.

AUTHOR CONTRIBUTIONS

Conceived and designed research: M.L.C. and A.A.M. Performed experiments: M.L.C., A.D.S., J.W.N. Analyzed data: M.L.C., A.D.S., A.A.M. Interpreted results: M.L.C. and A.A.M. Prepared figures: M.L.C. and A.A.M. Drafted manuscript: M.L.C. Edited and revised manuscript, M.L.C., A.D.S., J.W.N., and A.A.M. Approved final version of manuscript: M.L.C., A.D.S., J.W.N., and A.A.M.

686
687

REFERENCES

688 1. **Strange K, Emma F and Jackson PS**. Cellular and molecular physiology of volume-
689 sensitive anion channels. *Am J Physiol* 270: C711-C730, 1996.

690 2. **Okada Y**. Volume expansion-sensing outward-rectifier Cl- channel: fresh start to the
691 molecular identity and volume sensor. *Am J Physiol Cell Physiol* 273: C755-C789, 1997.
692 doi: 10.1152/ajpcell.1997.273.3.C755

693 3. **Nilius B, Eggermont J, Voets T, Buyse G, Manolopoulos V and Droogmans G**.
694 Properties of volume-regulated anion channels in mammalian cells. *Prog Biophys Mol*
695 *Biol* 68: 69-119, 1997.

696 4. **Hazama A and Okada Y**. Ca2+ sensitivity of volume-regulatory K+ and Cl- channels in
697 cultured human epithelial cells. *J Physiol* 402: 687-702, 1988.

698 5. **Cahalan MD and Lewis RS**. Role of potassium and chloride channels in volume
699 regulation by T lymphocytes. *Soc Gen Physiol Ser* 43: 281-301, 1988. doi: n/a

700 6. **Worrell RT, Butt AG, Cliff WH and Frizzell RA**. A volume-sensitive chloride
701 conductance in human colonic cell line T84. *Am J Physiol* 256: C1111-C1119, 1989.

702 7. **Solc CK and Wine JJ**. Swelling-induced and depolarization-induced C1-channels in
703 normal and cystic fibrosis epithelial cells. *Am J Physiol* 261: C658-C674, 1991. doi:
704 10.1152/ajpcell.1991.261.4.C658

705 8. **Kimelberg HK, Goderie SK, Higman S, Pang S and Waniewski RA**. Swelling-induced
706 release of glutamate, aspartate, and taurine from astrocyte cultures. *J Neurosci* 10:
707 1583-1591, 1990.

708 9. **Roy G and Malo C**. Activation of amino acid diffusion by a volume increase in cultured
709 kidney (MDCK) cells. *J Membr Biol* 130: 83-90, 1992.

710 10. **Kirk K, Ellory JC and Young JD**. Transport of organic substrates via a volume-
711 activated channel. *J Biol Chem* 267: 23475-23478, 1992.

712 11. **Jackson PS and Strange K**. Volume-sensitive anion channels mediate swelling-
713 activated inositol and taurine efflux. *Am J Physiol* 265: C1489-C1500, 1993. doi:
714 10.1152/ajpcell.1993.265.6.C1489

715 12. **Eggermont J, Trouet D, Carton I and Nilius B**. Cellular function and control of volume-
716 regulated anion channels. *Cell Biochem Biophys* 35: 263-274, 2001.

717 13. **Mongin AA**. Volume-regulated anion channel--a frenemy within the brain. *Pflugers Arch*
718 468: 421-441, 2016.

719 14. **Jentsch TJ**. VRACs and other ion channels and transporters in the regulation of cell
720 volume and beyond. *Nat Rev Mol Cell Biol* 17: 293-307, 2016.

721 15. **Chen L, Konig B, Liu T, Pervaiz S, Razzaque YS and Stauber T**. More than just a
722 pressure relief valve: physiological roles of volume-regulated LRRC8 anion channels.
723 *Biol Chem* 400: 1481-1496, 2019. doi: 10.1515/hsz-2019-0189

724 16. **Okada Y**. Physiology of the volume-sensitive/regulatory anion channel VSOR/VRAC:
725 part 2: its activation mechanisms and essential roles in organic signal release. *J Physiol*
726 *Sci* 74: 34, 2024. doi: 10.1186/s12576-023-00897-x

727 17. **Kimelberg HK**. Astrocytic swelling in cerebral ischemia as a possible cause of injury
728 and target for therapy. *Glia* 50: 389-397, 2005.

729 18. **Mongin AA**. Disruption of ionic and cell volume homeostasis in cerebral ischemia: The
730 perfect storm. *Pathophysiology* 14: 183-193, 2007.

731 19. **Akita T and Okada Y**. Characteristics and roles of the volume-sensitive outwardly
732 rectifying (VSOR) anion channel in the central nervous system. *Neuroscience* 275: 211-
733 231, 2014.

734 20. **Hyzinski-Garcia MC, Rudkouskaya A and Mongin AA**. LRRC8A protein is
735 indispensable for swelling-activated and ATP-induced release of excitatory amino acids
736 in rat astrocytes. *J Physiol* 592: 4855-4862, 2014.

737 21. **Lutter D, Ullrich F, Lueck JC, Kempa S and Jentsch TJ**. Selective transport of
738 neurotransmitters and modulators by distinct volume-regulated LRRC8 anion channels.
739 *J Cell Sci* 130: 1122-1133, 2017.

740 22. **Mongin AA and Kimelberg HK**. Astrocytic swelling in neuropathology. In: *Neuroglia*,
741 edited by Kettenmann H and Ransom BR. Oxford/New York: Oxford University Press,
742 2005.

743 23. **Wilson CS and Mongin AA**. Cell volume control in healthy brain and neuropathologies.
744 *Curr Top Membr* 81: 385-455, 2018.

745 24. **Kimelberg HK, Feustel PJ, Jin Y, Paquette J, Boulos A, Keller RW, Jr. and Tranmer**
746 **BI**. Acute treatment with tamoxifen reduces ischemic damage following middle cerebral
747 artery occlusion. *Neuroreport* 11: 2675-2679, 2000.

748 25. **Kimelberg HK, Jin Y, Charniga C and Feustel PJ**. Neuroprotective activity of
749 tamoxifen in permanent focal ischemia. *J Neurosurg* 99: 138-142, 2003.

750 26. **Zhang Y, Zhang H, Feustel PJ and Kimelberg HK**. DCPIB, a specific inhibitor of
751 volume regulated anion channels (VRACs), reduces infarct size in MCAo and the
752 release of glutamate in the ischemic cortical penumbra. *Exp Neurol* 210: 514-520, 2008.

753 27. **Boulos AS, Deshaies EM, Dalfino JC, Feustel PJ, Popp AJ and Drazin D**. Tamoxifen
754 as an effective neuroprotectant in an endovascular canine model of stroke. *J Neurosurg*
755 114: 1117-1126, 2011.

28. **Chen J, Yang J, Chu J, Chen KH, Alt J, Rais R and Qiu Z**. The SWELL1 channel promotes ischemic brain damage by mediating neuronal swelling and glutamate toxicity. *Adv Sci (Weinh)* 11: e2401085, 2024. doi: 10.1002/advs.202401085

29. **Pedersen SF, Okada Y and Nilius B**. Biophysics and physiology of the volume-regulated anion channel (VRAC)/volume-sensitive outwardly rectifying anion channel (VSOR). *Pflugers Arch* 468: 371-383, 2016.

30. **Strange K, Yamada T and Denton JS**. A 30-year journey from volume-regulated anion currents to molecular structure of the LRRC8 channel. *J Gen Physiol* 151: 100-117, 2019.

31. **Okada Y**. Physiology of the volume-sensitive/regulatory anion channel VSOR/VRAC. Part 1: from its discovery and phenotype characterization to the molecular entity identification. *J Physiol Sci* 74: 3, 2024. doi: 10.1186/s12576-023-00897-x

32. **Qiu Z, Dubin AE, Mathur J, Tu B, Reddy K, Miraglia LJ, Reinhardt J, Orth AP and Patapoutian A**. SWELL1, a plasma membrane protein, is an essential component of volume-regulated anion channel. *Cell* 157: 447-458, 2014.

33. **Voss FK, Ullrich F, Munch J, Lazarow K, Lutter D, Mah N, Andrade-Navarro MA, von Kries JP, Stauber T and Jentsch TJ**. Identification of LRRC8 heteromers as an essential component of the volume-regulated anion channel VRAC. *Science* 344: 634-638, 2014. doi: 10.1126/science.1252826

34. **Abascal F and Zardoya R**. LRRC8 proteins share a common ancestor with pannexins, and may form hexameric channels involved in cell-cell communication. *Bioessays* 34: 551-560, 2012.

35. **Syeda R, Qiu Z, Dubin AE, Murthy SE, Florendo MN, Mason DE, Mathur J, Cahalan SM, Peters EC, Montal M and Patapoutian A**. LRRC8 proteins form volume-regulated anion channels that sense ionic strength. *Cell* 164: 499-511, 2016. doi: 10.1016/j.cell.2015.12.031

36. **Deneka D, Sawicka M, Lam AKM, Paulino C and Dutzler R**. Structure of a volume-regulated anion channel of the LRRC8 family. *Nature* 558: 254-259, 2018.

37. **Kasuya G, Nakane T, Yokoyama T, Jia Y, Inoue M, Watanabe K, Nakamura R, Nishizawa T, Kusakizako T, Tsutsumi A, Yanagisawa H, Dohmae N, Hattori M, Ichijo H, Yan Z, Kikkawa M, Shirouzu M, Ishitani R and Nureki O**. Cryo-EM structures of the human volume-regulated anion channel LRRC8. *Nat Struct Mol Biol* 25: 797-804, 2018.

38. **Kefauver JM, Saotome K, Dubin AE, Pallesen J, Cottrell CA, Cahalan SM, Qiu Z, Hong G, Crowley CS, Whitwam T, Lee WH, Ward AB and Patapoutian A**. Structure of the human volume regulated anion channel. *eLife* 7: e38461, 2018.

792 39. **Kern DM, Oh S, Hite RK and Brohawn SG**. Cryo-EM structures of the DCPIB-inhibited
793 volume-regulated anion channel LRRC8A in lipid nanodiscs. *eLife* 8: e42636, 2019. doi:
794 10.7554/eLife.42636

795 40. **Rutz S, Deneka D, Dittmann A, Sawicka M and Dutzler R**. Structure of a volume-
796 regulated heteromeric LRRC8A/C channel. *Nat Struct Mol Biol* 30: 52-61, 2023.

797 41. **Takahashi H, Yamada T, Denton JS, Strange K and Karakas E**. Cryo-EM structures
798 of an LRRC8 chimera with native functional properties reveal heptameric assembly.
799 *eLife* 12: e82431, 2023. doi: 10.7554/eLife.82431

800 42. **Kumar L, Chou J, Yee CS, Borzutzky A, Vollmann EH, von Andrian UH, Park SY,**
801 **Hollander G, Manis JP, Poliani PL and Geha RS**. Leucine-rich repeat containing 8A
802 (LRRC8A) is essential for T lymphocyte development and function. *J Exp Med* 211: 929-
803 942, 2014.

804 43. **Sawada A, Takihara Y, Kim JY, Matsuda-Hashii Y, Tokimasa S, Fujisaki H, Kubota**
805 **K, Endo H, Onodera T, Ohta H, Ozono K and Hara J**. A congenital mutation of the
806 novel gene LRRC8 causes agammaglobulinemia in humans. *J Clin Invest* 112: 1707-
807 1713, 2003.

808 44. **Yang J, Vitery MDC, Chen J, Osei-Owusu J, Chu J and Qiu Z**. Glutamate-releasing
809 SWELL1 channel in astrocytes modulates synaptic transmission and promotes brain
810 damage in stroke. *Neuron* 102: 813-827, 2019.

811 45. **Yang J, Chen J, Liu Y, Chen KH, Baraban JM and Qiu Z**. Ventral tegmental area
812 astrocytes modulate cocaine reward by tonically releasing GABA. *Neuron* 2023.

813 46. **Zhou JJ, Luo Y, Chen SR, Shao JY, Sah R and Pan HL**. LRRC8A-dependent volume-
814 regulated anion channels contribute to ischemia-induced brain injury and glutamatergic
815 input to hippocampal neurons. *Exp Neurol* 332: 113391, 2020.

816 47. **Wilson CS, Dohare P, Orbeta S, Nalwalk JW, Huang Y, Ferland RJ, Sah R, Scimemi**
817 **A and Mongin AA**. Late adolescence mortality in mice with brain-specific deletion of the
818 volume-regulated anion channel subunit LRRC8A. *FASEB J* 35: e21869, 2021.

819 48. **Balkaya M, Dohare P, Chen S, Schober AL, Fidaleo AM, Nalwalk JW, Sah R and**
820 **Mongin AA**. Conditional deletion of LRRC8A in the brain reduces stroke damage
821 independently of swelling-activated glutamate release. *iScience* 26: 106669, 2023. doi:
822 10.1016/j.isci.2023.106669

823 49. **Planells-Cases R, Lutter D, Guyader C, Gerhards NM, Ullrich F, Elger DA,**
824 **Kucukosmanoglu A, Xu G, Voss FK, Reincke SM, Stauber T, Blomen VA, Vis DJ,**
825 **Wessels LF, Brummelkamp TR, Borst P, Rottenberg S and Jentsch TJ**. Subunit
826 composition of VRAC channels determines substrate specificity and cellular resistance
827 to Pt-based anti-cancer drugs. *EMBO J* 34: 2993-3008, 2015.

828 50. **Schober AL, Wilson CS and Mongin AA**. Molecular composition and heterogeneity of
829 the LRRC8-containing swelling-activated osmolyte channels in primary rat astrocytes. *J*
830 *Physiol* 595: 6939-6951, 2017.

831 51. **Gaitan-Penas H, Gradogna A, Laparra-Cuervo L, Solsona C, Fernandez-Duenas V,**
832 **Barrallo-Gimeno A, Ciruela F, Lakadamyali M, Pusch M and Estevez R**. Investigation
833 of LRRC8-mediated volume-regulated anion currents in Xenopus oocytes. *Biophys J*
834 111: 1429-1443, 2016.

835 52. **Livak KJ and Schmittgen TD**. Analysis of relative gene expression data using real-time
836 quantitative PCR and the 2(-Delta Delta C(T)) Method. *Methods* 25: 402-408, 2001.

837 53. **Schneider CA, Rasband WS and Eliceiri KW**. NIH Image to ImageJ: 25 years of
838 image analysis. *Nat Methods* 9: 671-675, 2012.

839 54. **Abdullaev IF, Rudkouskaya A, Schools GP, Kimelberg HK and Mongin AA**.
840 Pharmacological comparison of swelling-activated excitatory amino acid release and Cl-
841 currents in rat cultured astrocytes. *J Physiol* 572: 677-689, 2006. doi:
842 10.1113/jphysiol.2005.103820

843 55. **Bowens NH, Dohare P, Kuo YH and Mongin AA**. DCPIB, the proposed selective
844 blocker of volume-regulated anion channels, inhibits several glutamate transport
845 pathways in glial cells. *Mol Pharmacol* 83: 22-32, 2013. doi: 10.1124/mol.112.080457

846 56. **Schober AL and Mongin AA**. Intracellular levels of glutamate in swollen astrocytes are
847 preserved via neurotransmitter reuptake and de novo synthesis: implications for
848 hyponatremia. *J Neurochem* 135: 176-185, 2015.

849 57. **Tronche F, Kellendonk C, Kretz O, Gass P, Anlag K, Orban PC, Bock R, Klein R**
850 **and Schutz G**. Disruption of the glucocorticoid receptor gene in the nervous system
851 results in reduced anxiety. *Nat Genet* 23: 99-103, 1999.

852 58. **Dubois NC, Hofmann D, Kaloulis K, Bishop JM and Trumpp A**. Nestin-Cre
853 transgenic mouse line Nes-Cre1 mediates highly efficient Cre/loxP mediated
854 recombination in the nervous system, kidney, and somite-derived tissues. *Genesis* 44:
855 355-360, 2006.

856 59. **Liu HT, Tashmukhamedov BA, Inoue H, Okada Y and Sabirov RZ**. Roles of two
857 types of anion channels in glutamate release from mouse astrocytes under ischemic or
858 osmotic stress. *Glia* 54: 343-357, 2006.

859 60. **Sabirov RZ, Merzlyak PG, Okada T, Islam MR, Uramoto H, Mori T, Makino Y,**
860 **Matsuura H, Xie Y and Okada Y**. The organic anion transporter SLCO2A1 constitutes
861 the core component of the Maxi-Cl channel. *EMBO J* 36: 3309-3324, 2017.

862 61. **Woo DH, Han KS, Shim JW, Yoon BE, Kim E, Bae JY, Oh SJ, Hwang EM,**
863 **Marmorstein AD, Bae YC, Park JY and Lee CJ**. TREK-1 and Best1 channels mediate

fast and slow glutamate release in astrocytes upon GPCR activation. *Cell* 151: 25-40, 2012.

62. **Oh SJ, Han KS, Park H, Woo DH, Kim HY, Traynelis SF and Lee CJ**. Protease activated receptor 1-induced glutamate release in cultured astrocytes is mediated by Bestrophin-1 channel but not by vesicular exocytosis. *Mol Brain* 5: 38, 2012.

63. **Han YE, Kwon J, Won J, An H, Jang MW, Woo J, Lee JS, Park MG, Yoon BE, Lee SE, Hwang EM, Jung JY, Park H, Oh SJ and Lee CJ**. Tweety-homolog (Ttyh) family encodes the pore-forming subunits of the swelling-dependent volume-regulated anion channel (VRAC(swell)) in the brain. *Exp Neurobiol* 28: 183-215, 2019. doi: 10.5607/en.2019.28.2.183

64. **Ye ZC, Wyeth MS, Baltan-Tekkok S and Ransom BR**. Functional hemichannels in astrocytes: a novel mechanism of glutamate release. *J Neurosci* 23: 3588-3596, 2003.

65. **Duan S, Anderson CM, Keung EC, Chen Y, Chen Y and Swanson RA**. P2X7 receptor-mediated release of excitatory amino acids from astrocytes. *J Neurosci* 23: 1320-1328, 2003.

66. **Iglesias R, Dahl G, Qiu F, Spray DC and Scemes E**. Pannexin 1: the molecular substrate of astrocyte "hemichannels". *J Neurosci* 29: 7092-7097, 2009.

67. **Pervaiz S, Kopp A, von KL and Stauber T**. Absolute protein amounts and relative abundance of volume-regulated anion channel (VRAC) LRRC8 subunits in cells and tissues revealed by quantitative immunoblotting. *Int J Mol Sci* 20: 5879, 2019. doi: 10.3390/ijms20235879

68. **Knecht DA, Zeziulia M, Bhavsar MB, Puchkov D, Maier H and Jentsch TJ**. LRRC8/VRAC volume-regulated anion channels are crucial for hearing. *J Biol Chem* 300: 107436, 2024. doi: 10.1016/j.jbc.2024.107436

69. **Concepcion AR, Wagner LE, Zhu J, Tao AY, Yang J, Khodadadi-Jamayran A, Wang YH, Liu M, Rose RE, Jones DR, Coetzee WA, Yule DI and Feske S**. The volume-regulated anion channel LRRC8C suppresses T cell function by regulating cyclic dinucleotide transport and STING-p53 signaling. *Nat Immunol* 23: 287-302, 2022. doi: 10.1038/s41590-021-01105-x

70. **Yanushkevich S, Zieminska A, Gonzalez J, Anazco F, Song R, Arias-Cavieres A, Granados ST, Zou J, Rao Y and Concepcion AR**. Recent advances in the structure, function and regulation of the volume-regulated anion channels and their role in immunity. *J Physiol* 2024. doi: 10.1113/JP285200

71. **Ghosh A, Khandelwal N, Kumar A and Bera AK**. Leucine-rich repeat-containing 8B protein is associated with the endoplasmic reticulum Ca(2+) leak in HEK293 cells. *J Cell Sci* 130: 3818-3828, 2017.

72. **Quinodoz M, Rutz S, Peter V, Garavelli L, Innes AM, Lehmann EF, Kellenberger S, Peng Z, Barone A, Campos-Xavier B, Unger S, Rivolta C, Dutzler R and Superti-Furga A**. De novo variants in LRRC8C resulting in constitutive channel activation cause a human multisystem disorder. *EMBO J* 44: 413-436, 2025. doi: 10.1038/s44318-024-00322-y

FIGURE LEGENDS

Figure 1: LRRC8A-containing VRACs are the main conduit for swelling-activated release of cytosolic glutamate.

A1, Breeding strategy for brain-specific deletion of LRRC8A using *Nestin*^{Cre} recombination. The four genotypes generated are: *Lrrc8a*$^{flox/+}$ (fl/+), *Lrrc8a*$^{flox/flox}$ (fl/fl), *Lrrc8a*$^{flox/+}$:*Nestin*$^{Cre/+}$ (HET), and *Lrrc8a*$^{flox/flox}$:*Nestin*$^{Cre/+}$ (KO). **A2**, Representative live image of LRRC8A HET astrocytes expressing the Cre reporter Ai9. TdTomato fluorescence was captured at 320× magnification. **B**, Western blot analysis of LRRC8A expression in primary astrocyte cultures from the four genotypes shown in (A1). **B1**, Representative full-length Western blot of LRRC8A immuno-reactivity and matching β-actin signal probed on the same membrane. **B2**, Quantification of LRRC8A expression normalized to β-actin and presented relative to the average signal from fl/+ samples. Data are the mean values ± SD from five cultures per group. ****p <0.0001, one-way ANOVA with Tukey's multiple comparisons test. **C**, VRAC activity in primary astrocytes assessed as swelling-activated release of D-[^{3}H]aspartate in response to a 30% reduction in medium osmolality (290 to 200 mOsm). Data are the means ± SD from 8–16 independent experiments in at least two different astrocyte cultures per genotype. *p < 0.05, ****p < 0.0001, HET (n=8) and KO (n=8) vs. controls (fl/+ and fl/fl, n=16), respectively. $^{\#\#}$p < 0.01, HET vs. KO. One-way ANOVA of maximal release values with Tukey's multiple comparisons test. **Inset:** Hypoosmotic response in LRRC8A KO astrocytes shown on an expanded scale. **D**, VRAC activity in primary astrocytes exposed to a 50% reduction in medium osmolality (from 290 to 150 mOsm). Data are the means ± SD from 8–11 independent experiments in at least two different astrocyte cultures per genotype. ****p < 0.0001, HET (n=9) and KO (n=8) vs. controls (fl/+ and fl/fl, n=11); $^{\#}$p < 0.05, HET vs. KO. One-way ANOVA with Tukey's multiple comparisons test. **Inset:** Hypoosmotic response in LRRC8A KO astrocytes shown on an expanded scale.

Figure 2: Relative abundance of *Lrrc8a-e* transcripts in mouse brain and primary astrocyte cultures.

A, Quantification of mRNA expression levels for *Lrrc8a–e* in mouse forebrain lysates using qRT-PCR. Expression levels were normalized to ribosomal *Rpl13a* within the same sample. Data are the means ± SD of 7 mouse forebrains. **B**, RNA-seq analysis of *Lrrc8a-e* expression in 7 mouse forebrain regions from 5 mice of both sexes (data downloaded from the Human Protein Atlas). **C**, Quantification of mRNA expression levels for *Lrrc8a–e* in primary astrocyte cultures measured with qRT-PCR and normalized to ribosomal *Rpl13a*. Data are the means ± SD of 6 independent cultures.

Figure 3: Functional contribution of individual LRRC8A-E subunits to glutamate-permeable VRACs.

A1, Quantification of *Lrrc8a-e* mRNA expression levels in mouse astrocyte cultures treated with negative control siRNA (siNC). Expression levels were normalized to the housekeeping *Rpl13a*.

946 Data are the means ± SD of 4 independently prepared cell cultures. **A2**, Schematic of a radiotracer
947 assay of VRAC activity (created with BioRender.com, see Methods for additional details). **B-F**,
948 Effects of gene-specific siRNA constructs on *Lrrc8a-e* mRNA expression levels 48 h post-
949 transfection and swelling-activated D-[^{3}H]aspartate release 96 h post transfection. ***B1-F1***, Relative
950 *Lrrc8a-e* expression was normalized to *Rpl13a* and compared to siNC. Values are the means ±
951 SD of 3-4 independent transfections in at least two different astrocyte cultures. *p<0.05, **p<0.01,
952 ***p<0.001, one-population t-test with Bonferroni correction for multiple comparisons. ***B2-F2***,
953 Integral D-[^{3}H]aspartate release values in cells exposed for 10 min to either isoosmotic (Basal) or
954 hypoosmotic (Hypo) conditions (see Methods). With the exception of *F2*, data are the means ±
955 SD of 6-9 independent transfections in two independently prepared cell cultures. For *Lrrc8e*
956 knockdowns in *F2*, data are the means ± SD of 3 independent transfections in one astrocyte
957 culture. ** p <0.01, *** p <0.001, ****p <0.0001, vs. siNC, repeated measures two-way ANOVA
958 with Tukey's multiple comparisons test (for clarity only the effect of siRNA under hypoosmotic
959 conditions are shown).

960

961 **Figure 4: Non-redundant roles of LRRC8C and LRRC8D subunits in glutamate-permeable**
962 **VRACs.**

963 **A**, Validation of siRNA efficacy in double knockdown experiments targeting *Lrrc8c* and *Lrrc8d*.
964 Astrocytes were treated with siRNA targeting *Lrrc8c* (siC1), *Lrrc8d* (siD4), or their combination
965 (siC1 + siD4). Efficacy of gene-specific knockdowns was verified by qRT-PCR. Data are the mean
966 normalized expression values ± SD in three independently transfected cell cultures. **p<0.01,
967 *p<0.05, one-population t-test with Bonferroni correction for multiple comparisons. **B**, Effect of
968 siC1, siD4, or siC1+siD4 on VRAC-mediated D-[^{3}H]aspartate release from cultured astrocytes
969 exposed to a 30% reduction in medium osmolality measured in a 12-well plate format. Data are
970 the means ± SD from 12 independent transfections in three different astrocyte cultures. ****p <
971 0.0001 vs. siNC, repeated measures two-way ANOVA with Tukey's multiple comparisons test
972 (only the effects of siRNAs under hypoosmotic conditions are shown). **C**, Kinetics of VRAC-
973 mediated D-[^{3}H]aspartate release from astrocyte cultures treated with siNC, siC1, or siC1+siD4
974 and exposed to a 30% reduction in medium osmolality. Data are the means ± SD in four-five
975 independent transfections. **Inset:** Statistical comparison of the maximal D-[^{3}H]aspartate release
976 values in the same experiments. *p<0.05, one-way ANOVA with Tukey's multiple comparisons
977 test. **D**, Kinetics of VRAC-mediated D-[^{3}H]aspartate release from astrocytes treated with siNC,
978 siC1, siD4, or siC1+siD4 and exposed to a 50% reduction in medium osmolality. Data are the
979 means ± SD in five-six independent transfections performed in two different astrocyte cultures.
980 **Inset:** Statistical comparison of the maximal D-[^{3}H]aspartate release values in the same
981 experiments. **p<0.01, ****p <0.0001, one-way ANOVA with Tukey's multiple comparisons test.

982

983 **Figure 5: Functional contribution of LRRC8B to LRRC8C- and LRRC8D-containing**
984 **VRACs.**

985 **A**, Validation of siRNA efficacy in double knockdown experiments targeting *Lrrc8b* and *Lrrc8c*.
986 Astrocytes were treated with siRNA targeting *Lrrc8b* (siB4), *Lrrc8c* (siC1), or their combination
987 (siB4+siC1). Efficacy of gene-specific knockdowns was verified by qRT-PCR. Data are the mean
988 normalized expression values ± SD in three independently transfected cell cultures. **p<0.01,
989 *p<0.05; one-population t-test with Bonferroni correction for multiple comparisons. **B**, Effects of

990 siNC, siB4, siC1, siB4+siC1 on VRAC-mediated D-[^{3}H]aspartate release from cultured astrocyte
991 exposed to a 30% reduction in medium osmolality, measured in a 12-well plate format. Data are
992 the means ± SD from 6 independent transfections in two different astrocyte cultures. ****p <
993 0.0001, repeated measures two-way ANOVA with Tukey's multiple comparisons test (only the
994 effects of siRNAs under hypoosmotic conditions are shown). **C**, qRT-PCR validation of double
995 siRNA knockdown experiments targeting *Lrrc8b* (siB4) and *Lrrc8d* (siD4). Astrocytes were treated
996 with siB4, siD4, or their combination (siB4+siD4). Data represent mean normalized expression
997 values ± SD in three-four independently transfected cell cultures. ***p<0.001, one-population t-
998 test with Bonferroni correction for multiple comparisons. **D**, Effects of siNC, siB4, siD4, siB4+siD4
999 on VRAC-mediated D-[^{3}H]aspartate release from cultured astrocyte exposed to a 30% reduction
1000 in medium osmolality measured in a 12-well plate format. Data are the means ± SD from 6
1001 independent transfections in two different astrocyte cultures. ***p<0.001, ****p<0.0001; repeated
1002 measures two-way ANOVA with Tukey's multiple comparisons test (only the effects of siRNAs
1003 under hypoosmotic conditions are shown).

1004

1005 **Figure 6: Proposed subunit composition of glutamate-permeable VRACs in astrocytes.**

1006 **A** and **B**, Theoretical predictions of the effects on siRNA knockdowns on VRAC activity based on
1007 two models of VRAC composition. In *Model I*, VRACs are assembled from LRRC8A, LRRC8C,
1008 and LRRC8D subunits, with LRRC8C and LRRC8D functioning as mutually redundant
1009 components. In *Model II*, two independent VRAC populations are formed by either LRRC8A+
1010 LRRC8C or LRRC8A+LRRC8D. In this case, LRRC8C and LRRC8D subunits are not functionally
1011 redundant. **C**, *Experimental outcomes* showing the effects of LRRC8C (siC) and/or LRRC8D (siD)
1012 knockdown on VRAC-mediated D-[^{3}H]aspartate release in mouse astrocytes subjected to
1013 moderate (30% reduction in osmolarity; light bars) or severe (50% reduction in osmolarity; dark
1014 bars) hypotonic stress. These results are consistent with the Model II in which two distinct VRAC
1015 populations (labeled 1 and 2) mediate glutamate permeability. Additional data in the manuscript
1016 indicate that LRRC8B likely plays a structural role in these channels. LRRC8A+LRRC8D-
1017 containing VRACs provide a smaller contribution to swelling-activated glutamate release and their
1018 activity is dependent on the degree of cellular swelling. ***p<0.001, *p=0.012; unpaired t-tests.

1019

1020 # TABLES

1021

1022 **Table 1.** List of molecular biology tools used in qRT-PCR analyses and RNAi experiments in this
1023 study.

Target gene	Catalogue # qPCR primers	siRNA name (catalogue #)	siRNA target sequence
Negative Control (NC)	N/A	AllStars NC (SI03650318)	Scrambled (proprietary)
Lrrc8a	QT01167502	Mm_Lrrc8_1 (SI01296127)	CAGCCTCAAGAAGATGGTTAA
		Mm_Lrrc8_3 (SI01296141)	CAGAGTCATCTCAGGGTTAAA
		Mm_Lrrc8_4 (SI01296148)	AATGATGGTTTGGGTATTAAA
Lrrc8b	QT01541666	Mm_LOC433926_1 (SI01235311)	AAGAAGATGGTCAATCTGAAA
		Mm_LOC433926_3 (SI01235325)	ATCCTGTTTGTCCTTATTATA
		Mm_LOC433926_4 (SI01235332)	TAGGAGGATGAACTTTCCTAA
Lrrc8c	QT01042881	Mm_E430036I04Rik_1 (SI00988799)	ATCGGAGTTCTGCAAAGTTTA
		Mm_E430036I04Rik_2 (SI00988806)	GAGAAGTAACATATACATATA
		Mm_E430036I04Rik_4 (SI00988820)	CACCTTATACTGGCTGTTCTA
Lrrc8d	QT02255085	LRRC5_1 (SI01296043)	TTGCAAGTTATTACAAGATAA
		LRRC5_2 (SI01296050)	CAGCATGACAATCCTGGACAA
		LRRC5_3 (SI01296057)	CTGCTAAAGTATATGATTAAA
		LRRC5_4 (SI01296064)	AAGCCCTGTTTGAGAAAGTAA
Lrrc8e	QT01046269	Mm_1810049O03Rik_1 (SI00806043)	CACATTTAGCTATGTAATAAA
		Mm_1810049O03Rik_2 (SI00806050)	CTGAAGGTGATCTGTGTTAAA
		Mm_1810049O03Rik_4 (SI00806064)	CCCAACAAGGATCAGCATATA
GAPDH	QT01658692	N/A	N/A
Rpl13a	QT00267197	N/A	N/A
RPS20	QT00251433	N/A	N/A

1024

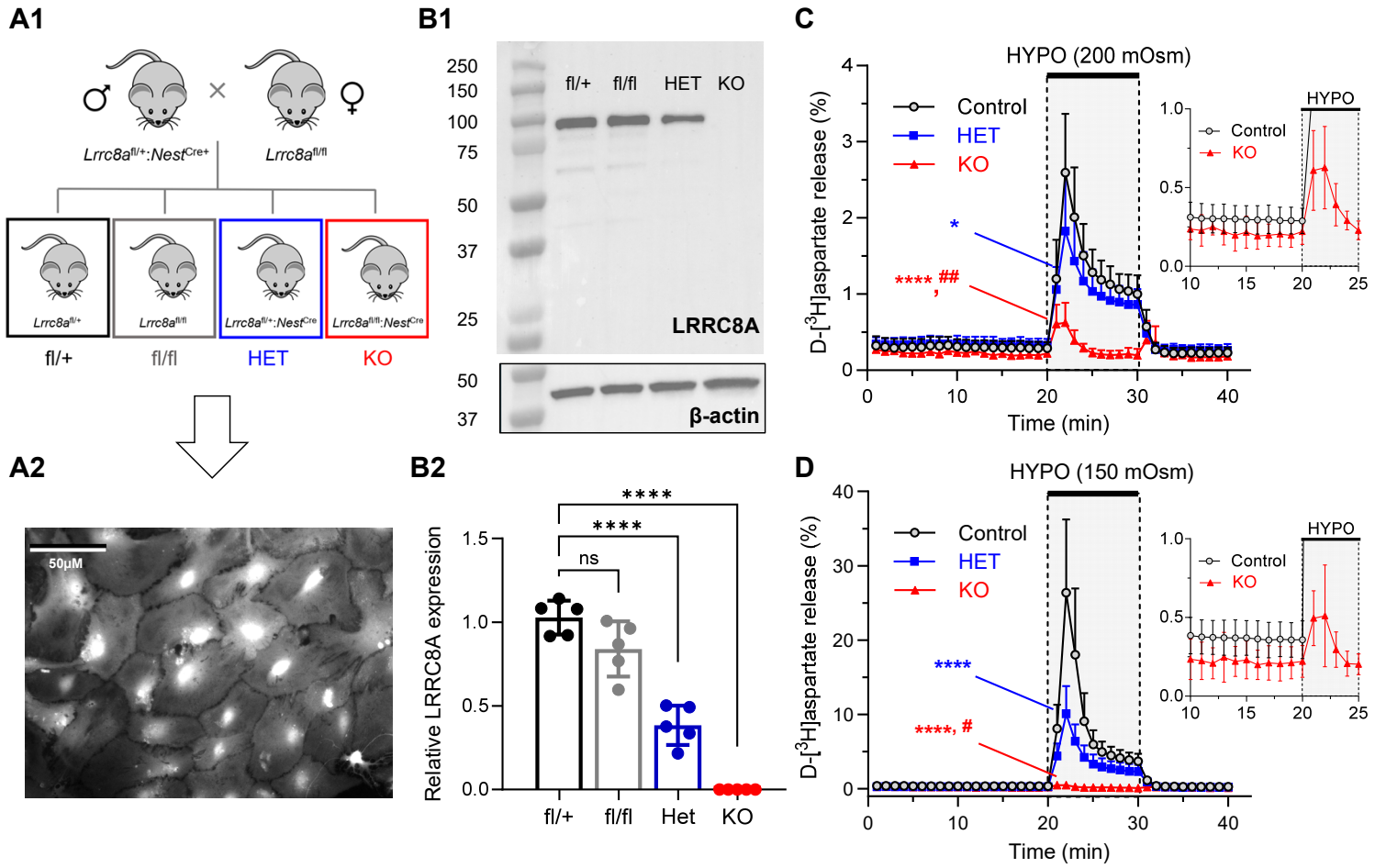

LRRC8A-containing VRACs are the main conduit for swelling-activated release of cytosolic glutamate.

A1, Breeding strategy for brain-specific deletion of LRRC8A using *Nestin*^{Cre} recombination. The four genotypes generated are: *Lrrc8a*$^{flox/+}$ (fl/+), *Lrrc8a*$^{flox/flox}$ (fl/fl), *Lrrc8a*$^{flox/+}$:*Nestin*$^{Cre/+}$ (HET), and *Lrrc8a*$^{flox/flox}$:*Nestin*$^{Cre/+}$ (KO). **A2**, Representative live image of LRRC8A HET astrocytes expressing the Cre reporter Ai9. TdTomato fluorescence was captured at 320× magnification. **B**, Western blot analysis of LRRC8A expression in primary astrocyte cultures from the four genotypes shown in (A1). **B1**, Representative full-length Western blot of LRRC8A immunoreactivity and matching β-actin signal probed on the same membrane. **B2**, Quantification of LRRC8A expression normalized to β-actin and presented relative to the average signal from fl/+ samples. Data are the mean values ± SD from five cultures per group. ****p <0.0001, one-way ANOVA with Tukey's multiple comparisons test. **C**, VRAC activity in primary astrocytes assessed as swelling-activated release of D-[^{3}H]aspartate in response to a 30% reduction in medium osmolality (290 to 200 mOsm). Data are the means ± SD from 8–16 independent experiments in at least two different astrocyte cultures per genotype. *p < 0.05, ****p < 0.0001, HET (n=8) and KO (n=8) vs. controls (fl/+ and fl/fl, n=16), respectively. $^{\#\#}$p < 0.01, HET vs. KO. One-way ANOVA of maximal release values with Tukey's multiple comparisons test. **Inset:** Hypoosmotic response in LRRC8A KO astrocytes shown on an expanded scale. **D**, VRAC activity in primary astrocytes exposed to a 50% reduction in medium osmolality (from 290 to 150 mOsm). Data are the means ± SD from 8–11 independent experiments in at least two different astrocyte cultures per genotype. ****p < 0.0001, HET (n=9) and KO (n=8) vs. controls (fl/+ and fl/fl, n=11); $^{\#}$p < 0.05, HET vs. KO. One-way ANOVA with Tukey's multiple comparisons test. **Inset:** Hypoosmotic response in LRRC8A KO astrocytes shown on an expanded scale.

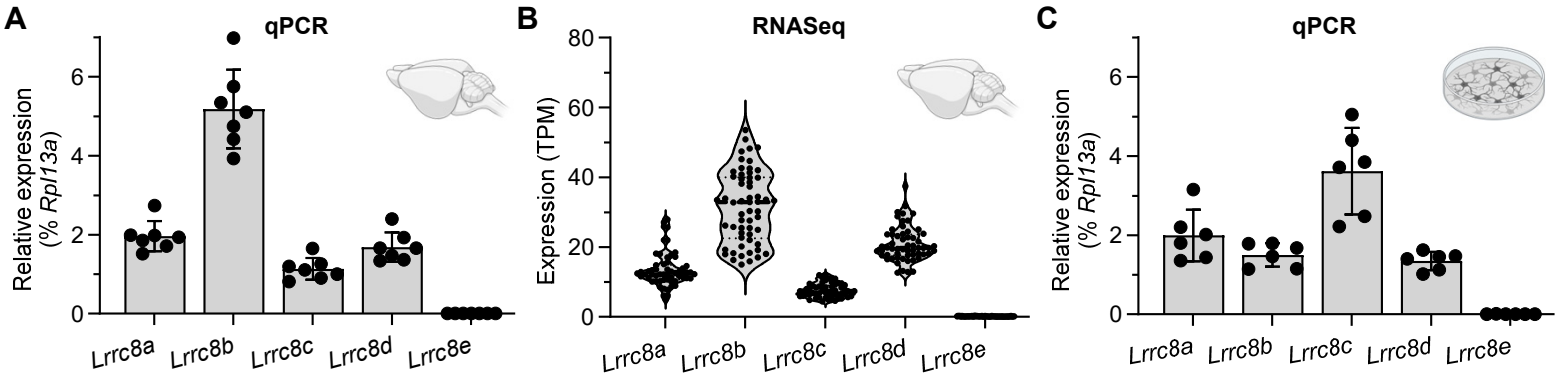

Relative abundance of *Lrrc8a-e* transcripts in mouse brain and primary astrocyte cultures.

A, Quantification of mRNA expression levels for *Lrrc8a–e* in mouse forebrain lysates using qRT-PCR. Expression levels were normalized to ribosomal *Rpl13a* within the same sample. Data are the means ± SD of 7 mouse forebrains. **B**, RNA-seq analysis of *Lrrc8a-e* expression in 7 mouse forebrain regions from 5 mice of both sexes (data downloaded from the Human Protein Atlas). **C**, Quantification of mRNA expression levels for *Lrrc8a–e* in primary astrocyte cultures measured with qRT-PCR and normalized to ribosomal *Rpl13a*. Data are the means ± SD of 6 independent cultures.

Figure 3 • M.L. Chandler *et al.*

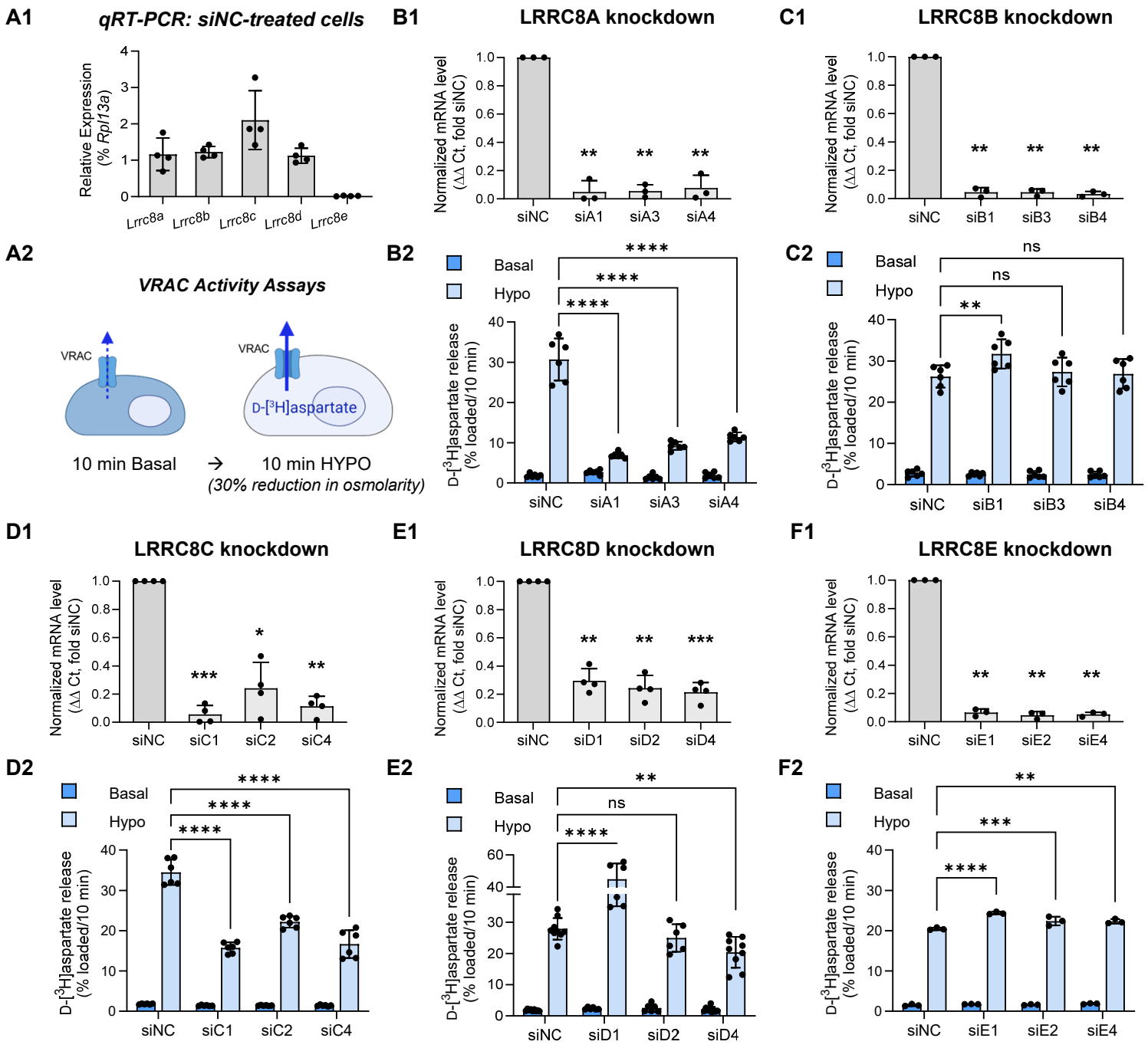

Functional contribution of individual LRRC8A-E subunits to glutamate-permeable VRACs.

A1, Quantification of *Lrrc8a-e* mRNA expression levels in mouse astrocyte cultures treated with negative control siRNA (siNC). Expression levels were normalized to the housekeeping gene *Rpl13a*. Data are the means ± SD of 4 independently prepared cell cultures. **A2**, Schematic of a radiotracer assay of VRAC activity (created with BioRender.com, see Methods for additional details). **B-F**, Effects of gene-specific siRNA constructs on *Lrrc8a-e* mRNA expression levels 48 h post-transfection and swelling-activated D-[^{3}H]aspartate release 96 h post-transfection. ***B1-F1***, Relative *Lrrc8a-e* expression was normalized to *Rpl13a* and compared to siNC. Values are the means ± SD of 3-4 independent transfections in at least two different astrocyte cultures. *p<0.05, **p<0.01, ***p<0.001, one-population t-test with Bonferroni correction for multiple comparisons. ***B2-F2***, Integral D-[^{3}H]aspartate release values in cells exposed for 10 min to either isoosmotic (Basal) or hypoosmotic (Hypo) conditions (see Methods). With the exception of *F2*, data are the means ± SD of 6-9 independent transfections in two independently prepared cell cultures. For *Lrrc8e* knockdowns in *F2*, data are the means ± SD of 3 independent transfections in one astrocyte culture. ** p <0.01, *** p <0.001, ****p <0.0001, vs. siNC, repeated measures two-way ANOVA with Tukey's multiple comparisons test (for clarity only the effect of siRNA under hypoosmotic conditions are shown).

Figure 4 • M.L. Chandler et al.

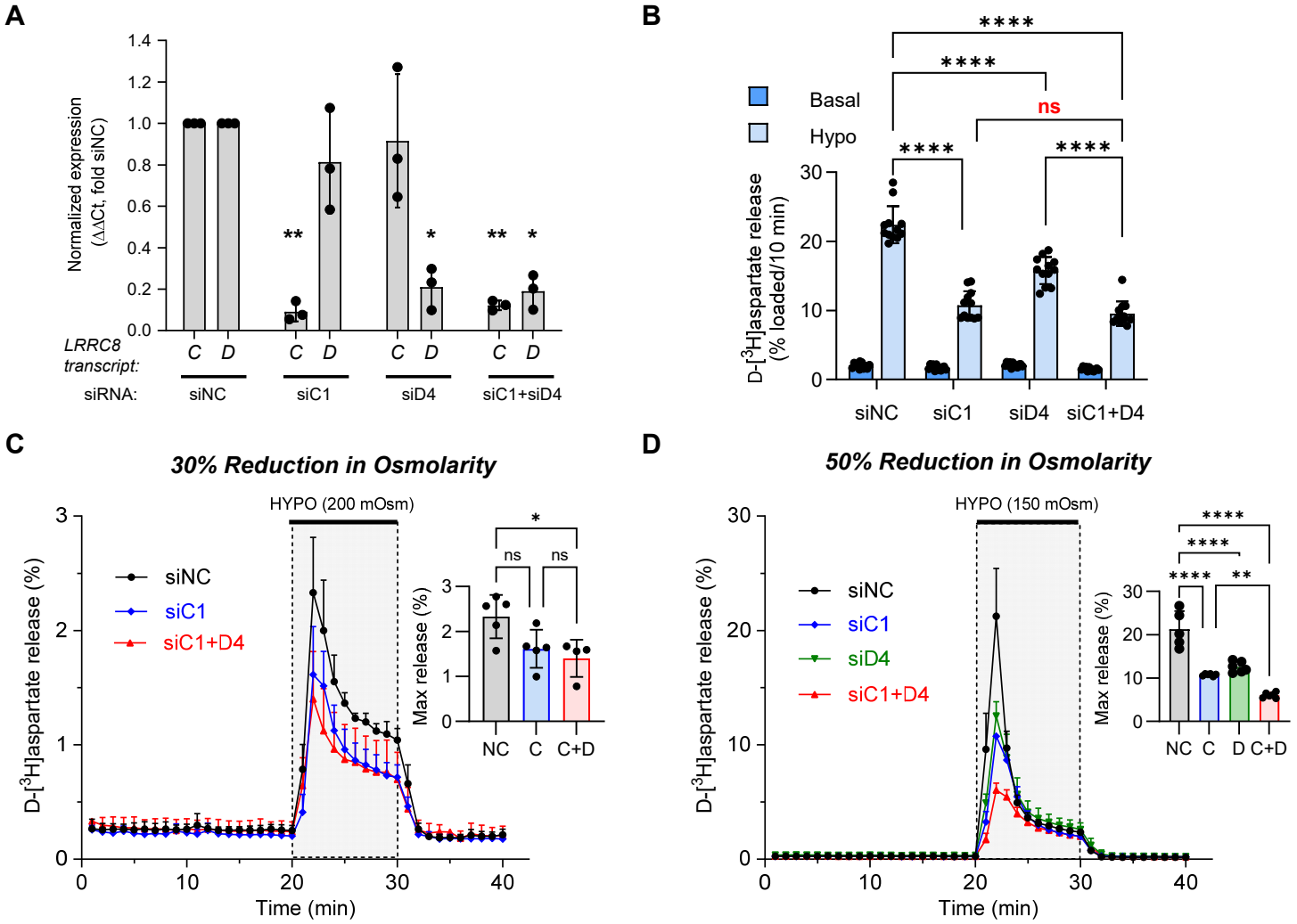

Non-redundant roles of LRRC8C and LRRC8D subunits in glutamate-permeable VRACs.

A, Validation of siRNA efficacy in double knockdown experiments targeting *Lrrc8c* and *Lrrc8d*. Astrocytes were treated with siRNA targeting *Lrrc8c* (siC1), *Lrrc8d* (siD4), or their combination (siC1 + siD4). Efficacy of gene-specific knockdowns was verified by qRT-PCR. Data are the mean normalized expression values ± SD in three independently transfected cell cultures. **p<0.01, *p<0.05, one-population t-test with Bonferroni correction for multiple comparisons. **B**, Effect of siC1, siD4, or siC1+siD4 on VRAC-mediated D-[^{3}H]aspartate release from cultured astrocytes exposed to a 30% reduction in medium osmolality measured in a 12-well plate format. Data are the means ± SD from 12 independent transfections in three different astrocyte cultures. ****p < 0.0001 vs. siNC, repeated measures two-way ANOVA with Tukey's multiple comparisons test (only the effects of siRNAs under hypoosmotic conditions are shown). **C**, Kinetics of VRAC-mediated D-[^{3}H]aspartate release from astrocyte cultures treated with siNC, siC1, or siC1+siD4 and exposed to a 30% reduction in medium osmolality. Data are the means ± SD in 4-5 independent transfections. **Inset:** Statistical comparison of the maximal D-[^{3}H]aspartate release values in the same experiments. *p<0.05, one-way ANOVA with Tukey's multiple comparisons test. **D**, Kinetics of VRAC-mediated D-[^{3}H]aspartate release from astrocytes treated with siNC, siC1, siD4, or siC1+siD4 and exposed to a 50% reduction in medium osmolality. Data are the means ± SD in 5-6 independent transfections performed in two different astrocyte cultures. **Inset:** Statistical comparison of the maximal D-[^{3}H]aspartate release values in the same experiments. **p<0.01, ****p <0.0001, one-way ANOVA with Tukey's multiple comparisons test.

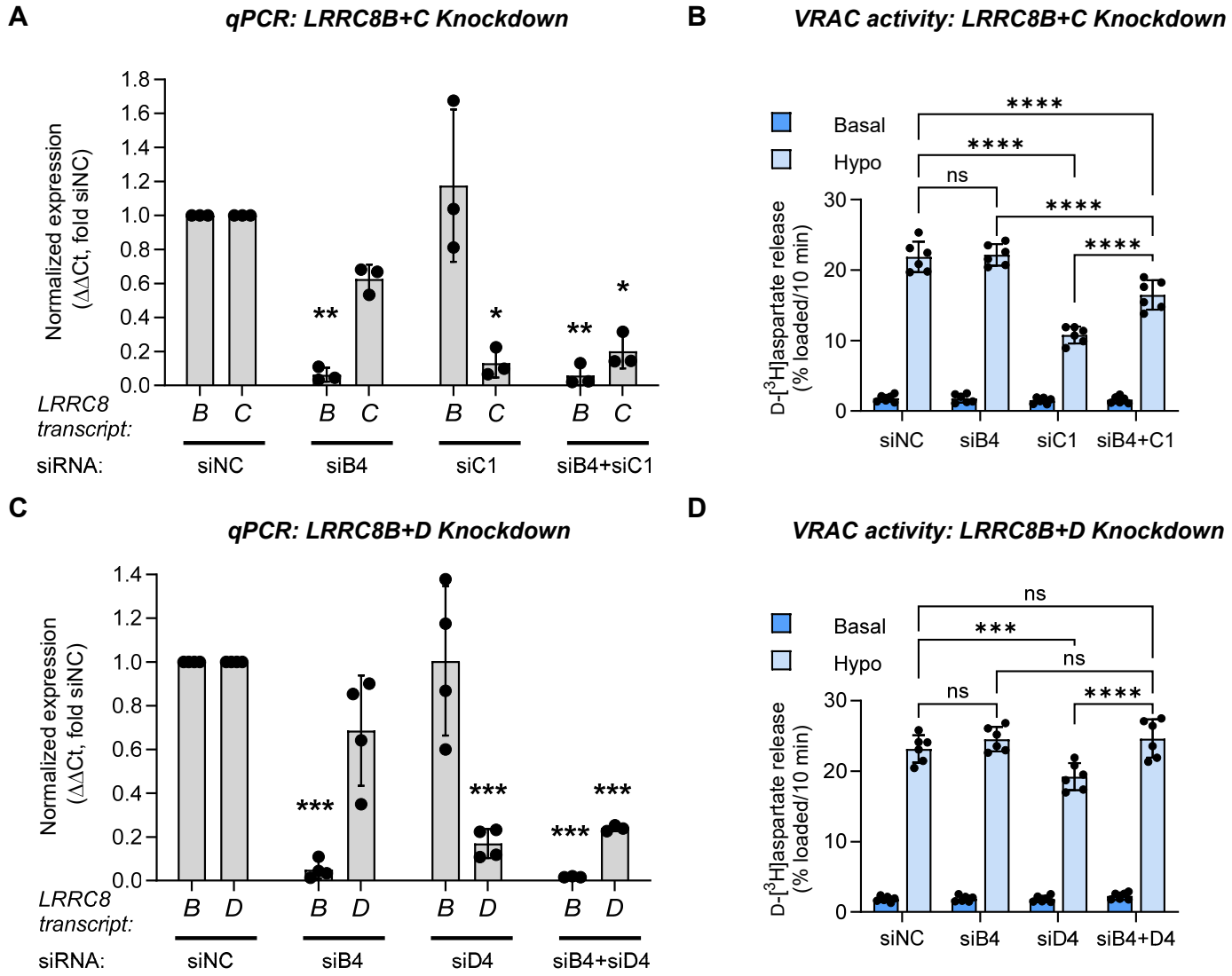

Functional contribution of LRRC8B to LRRC8C- and LRRC8D-containing VRACs.

A, Validation of siRNA efficacy in double knockdown experiments targeting *Lrrc8b* and *Lrrc8c*. Astrocytes were treated with siRNA targeting *Lrrc8b* (siB4), *Lrrc8c* (siC1), or their combination (siB4+siC1). Efficacy of gene-specific knockdowns was verified by qRT-PCR. Data are the mean normalized expression values ± SD in 3 independently transfected cell cultures. **p<0.01, *p<0.05; one-population t-test with Bonferroni correction for multiple comparisons. **B**, Effects of siNC, siB4, siC1, siB4+siC1 on VRAC-mediated D-[^{3}H]aspartate release from cultured astrocyte exposed to a 30% reduction in medium osmolality, measured in a 12-well plate format. Data are the means ± SD from 6 independent transfections in two different astrocyte cultures. ****p < 0.0001, repeated measures two-way ANOVA with Tukey's multiple comparisons test (only the effects of siRNAs under hypoosmotic conditions are shown). **C**, qRT-PCR validation of double siRNA knockdown experiments targeting *Lrrc8b* (siB4) and *Lrrc8d* (siD4). Astrocytes were treated with siB4, siD4, or their combination (siB4+siD4). Data represent mean normalized expression values ± SD in 3-4 independently transfected cell cultures. ***p<0.001, one-population t-test with Bonferroni correction for multiple comparisons. **D**, Effects of siNC, siB4, siD4, siB4+siD4 on VRAC-mediated D-[^{3}H]aspartate release from cultured astrocyte exposed to a 30% reduction in medium osmolality measured in a 12-well plate format. Data are the means ± SD from 6 independent transfections in two different astrocyte cultures. ***p < 0.001, ****p<0.0001; repeated measures two-way ANOVA with Tukey's multiple comparisons test (only the effects of siRNAs under hypoosmotic conditions are shown).

Figure 6 • M.L. Chandler et al.

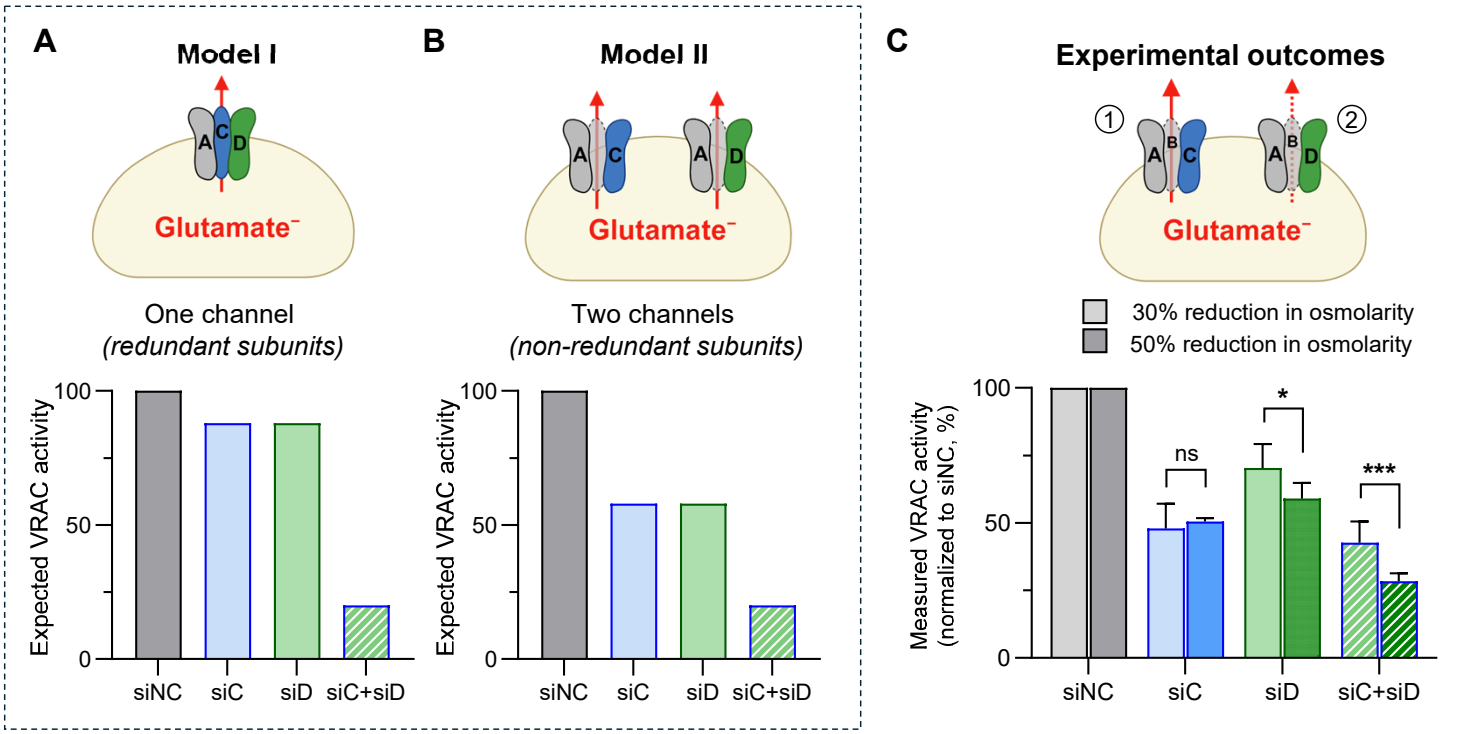

Proposed subunit composition of glutamate-permeable VRACs in astrocytes

A and **B**, Theoretical predictions of the effects on siRNA knockdowns on VRAC activity based on two models of VRAC composition. In *Model I*, VRACs are assembled from LRRC8A, LRRC8C, and LRRC8D subunits, with LRRC8C and LRRC8D functioning as mutually redundant components. In *Model II*, two independent VRAC populations are formed by either LRRC8A+LRRC8C or LRRC8A+LRRC8D. In this case, LRRC8C and LRRC8D subunits are not functionally redundant. **C**, *Experimental outcomes* showing the effects of LRRC8C (siC) and/or LRRC8D (siD) knockdown on VRAC-mediated D-[^{3}H]aspartate release in mouse astrocytes subjected to moderate (30% reduction in osmolarity; light bars) or severe (50% reduction in osmolarity; dark bars) hypotonic stress. These results are consistent with the Model II in which two distinct VRAC populations (labeled 1 and 2) mediate glutamate permeability. Additional data in the manuscript indicate that LRRC8B likely plays a structural role in these channels. LRRC8A+LRRC8D-containing VRACs provide a smaller contribution to swelling-activated glutamate release and their activity is dependent on the degree of cellular swelling. ***$p<0.001$, *$p=0.012$; unpaired t-tests.